BNL-222366-2021-JAAM

Selective Methane Oxidation to Methanol on ZnO/Cu2O/Cu(111) Catalysts: Multiple Site-dependent Behaviors

E. Huang, J. A. Rodriguez

To be published in "Journal of the American Chemical Society"

November 2021

Chemistry Department

Brookhaven National Laboratory

U.S. Department of Energy

USDOE Office of Science (SC), Basic Energy Sciences (BES) (SC-22)

DISCLAIMER

Selective Methane Oxidation to Methanol on $ZnO/Cu_2O/Cu(111)$ Catalysts: Multiple Site-dependent Behaviors

Erwei Huang[1,+], Ivan Orozco[1,+], Pedro J. Ramírez[2,3], Zongyuan Liu[4], Feng Zhang[5], Mausumi Mahapatra[4], Slavomír Nemšák[6], Sanjaya D. Senanayake[4,*], José A. Rodriguez[1,4,5,*], and Ping Liu[1,4*]

[1] Department of Chemistry, Stony Brook University, Stony Brook, NY 11794, (USA)

[2] Facultad de Ciencias, Universidad Central de Venezuela, Caracas 1020-A (Venezuela)

[3] Zoneca-CENEX, R&D Laboratories, Alta Vista, 64770 Monterrey (México)

[4] Chemistry Division, Brookhaven National Laboratory, Upton, NY 11973, (USA)

[5] Department of Materials Science and Engineering, Stony Brook University, Stony Brook, NY 11794, (USA)

[6] Advanced Light Source, Lawrence Berkeley National Laboratory, Berkeley, CA 94720, (USA)

[+] Co-first authors

[*] Corresponding authors: pingliu3@bnl.gov (P. L.), ssenanay@bnl.gov (S.D.S.) rodrigez@bnl.gov (J.A.R)

Abstract:

Due to the abundance of natural gas in our planet, a major goal is to achieve a direct methane to methanol conversion at medium to low temperatures using mixtures of methane and oxygen. Here, we report an efficient catalyst, $ZnO/Cu_2O/Cu(111)$, for this process investigated using a combination of reactor testing, scanning tunneling microscopy, ambient-pressure x-ray photoemission spectroscopy, density functional calculations, and kinetic Monte Carlo simulations. The catalyst is capable of methane activation at room temperature and transforms mixtures of methane and oxygen to methanol at 450 K with a selectivity of ~30%. This performance is not seen for other heterogenous catalysts which usually require the addition of water to enable a significant conversion of methane to methanol. The unique coarse structure of the ZnO islands supported on a $Cu_2O/Cu(111)$ substrate provides a collection of multiple centers that display different catalytic activity during the reaction. $ZnO\text{-}Cu_2O$ step sites are active centers for methanol synthesis when exposed to CH_4 and O_2 due to an effective O-O bond dissociation, which enables a methane-to-methanol conversion with a reasonable selectivity. Upon addition of water, the defected O-rich ZnO sites, introduced by Zn vacancies, show superior behavior towards methane conversion and enhance the overall methanol selectivity to over 80%. Thus, in this case, the surface sites involved in a direct $CH_4 \rightarrow CH_3OH$ conversion are different from those engaged in methanol formation without water. The identification of the site-dependent behavior of $ZnO/Cu_2O/Cu(111)$ opens a design strategy for guiding efficient methane reforming with high methanol selectivity.

1. Introduction

The high abundance of natural gas on the planet, with methane (CH_4) as its main component, has led to a strong interest in using this light alkane as a starting point or building block to produce high value chemicals[1-3]. In addition, since CH_4 is a potent greenhouse gas, there is a clear need to remove it or prevent its evolution into the atmosphere. The activation of CH_4 can be challenging due to the non-polar character of the molecule and the strength of its C-H bonds. Recent studies have shown advances in this direction when oxides, metal-oxide and metal-carbide interfaces are used for binding the light alkane and producing adsorbed CH_3 and CH_2 species at temperatures between 150 and 300 K[4-8]. Development of a catalyst for a direct conversion of CH_4 to methanol (CH_3OH) at medium to low temperatures using mixtures of methane and oxygen (O_2) can lead to a major commercial breakthrough in the utilization of the light alkane[1, 2, 9]. A limited oxidation of CH_4 to CH_3OH is difficult to achieve because the reaction has a thermodynamic tendency to yield carbon monoxide (CO) and/or carbon dioxide (CO_2) as final products[10].

To extract methanol in significant amounts, one needs materials that can activate CH_4 in an efficient way at temperatures below 500 K without decomposing CH_3O or other CH_xO intermediates[10]. A delicate balance involving the rates of reactions (1) and (2) is the key to achieve a selective conversion of methane to methanol[10].

$$CH_4 + 0.5O_2 \rightarrow CH_3OH \qquad (1)$$

$$CH_4 + 0.5O_2 \rightarrow CO + 3H_2 \qquad (2)$$

The enzyme methane monooxygenase transforms CH_4 into CH_3OH, working at 300 K and under limited or low concentrations of the reactants, but it cannot be employed for industrial-scale operations[11, 12]. In the enzyme, the synthesis of methanol is carried out by a set of three copper cations[12]. This fact has motivated many studies examining the performance of copper cations

presented in oxide lattices or dispersed inside zeolite frameworks[13-19]. Several of these systems produce methanol but only when water is used for extraction of the alcohol or when it is added to the reaction feed ($CH_4/O_2/H_2O$)[13-19]. In the case of Cu-exchanged zeolites, the process involves sequential steps of treatment in O_2, exposure to CH_4, and extraction with H_2O[13, 15-17, 20, 21]. On $CeO_x/Cu_2O/Cu(111)$ surfaces, a very good catalytic conversion of methane to methanol has been observed (~ 60% selectivity) in a single batch mode, but when water is removed from the reaction feed, the selectivity towards methanol formation is below 5%[18, 19]. Thus, there is a clear need to identify catalysts that can achieve the direct conversion of methane and O_2 to methanol.

In principle, the chemical environment around the copper cations can determine the relative rates of reactions (1) and (2). In this study, to enhance the performance of the $Cu_2O/Cu(111)$ substrate, we have switched from a CeO_x to a ZnO overlayer. Copper/zinc/aluminum oxide ($Cu/ZnO/Al_2O_3$) catalysts are widely used in the industry for methanol synthesis from CO and/or CO_2 hydrogenation[22]. Extensive studies have focused on understanding the nature of the active sites in $Cu/ZnO/Al_2O_3$ catalysts which in some cases seem to involve ZnO aggregates dispersed over particles of Cu or CuO_x [23-28]. These ZnO/Cu systems are not very aggressive towards CH_3O and CH_3OH species[22, 27, 29-31]. If these oxygenates form on top of ZnO/Cu surfaces, they should desorb as seen during CO_2 hydrogenation[22, 27, 31]. Besides CO/CO_2 hydrogenation to CH_3OH, Cu-ZnO interfaces are typically used for the water-gas shift[29] and CO oxidation reactions[30]. By comparison, the activation of CH_4 is more difficult due to the high stability of the alkane molecule[8].

The catalyst investigated in this study consists of large rough islands of ZnO dispersed on a $Cu_2O/Cu(111)$ substrate {$ZnO/Cu_2O/Cu(111)$, Figure 1}[31-33]. The ZnO islands have sizes in the range of 300-500 nm and expose surfaces which are rich in steps and contain either O or Zn vacancies. Thus, they offer different types of atomic arrays for the activation of small molecules.

[31-33] The behavior of these $ZnO/Cu_2O/Cu(111)$ systems and the reaction mechanism associated with CH_3OH synthesis were examined using scanning tunneling microscopy (STM), reactor testing, synchrotron-based ambient-pressure x-ray photoemission spectroscopy (AP-XPS), density functional theory (DFT) calculations, and kinetic Monte Carlo (KMC) simulations. Our objective is to present a detailed mechanistic study on a heterogenous catalyst that can selectively convert CH_4 to CH_3OH, which activates methane at room temperature, and achieves the transformation of the alkane into an alcohol under mild conditions (400-500 K). Indeed, the $ZnO/Cu_2O/Cu(111)$ surfaces display an activity for the direct $CH_4 \rightarrow CH_3OH$ process not seen for other heterogeneous catalysts reported in the literature[15-19, 34]. Overall, the superior catalytic performance of $ZnO/Cu_2O/Cu(111)$ originates in the roughness of the ZnO islands and strong $ZnO\text{-}Cu_2O$ interactions at the interface. Surface sites involved in the direct $CH_4 \rightarrow CH_3OH$ conversion are different from those engaged in methanol formation under the presence of water. Our study points to the role of new types of active sites and thus new ways in which the widely used Cu-ZnO catalysts could go beyond conventional CO_2 hydrogenation and perform a more challenging selective conversion of CH_4 to CH_3OH.

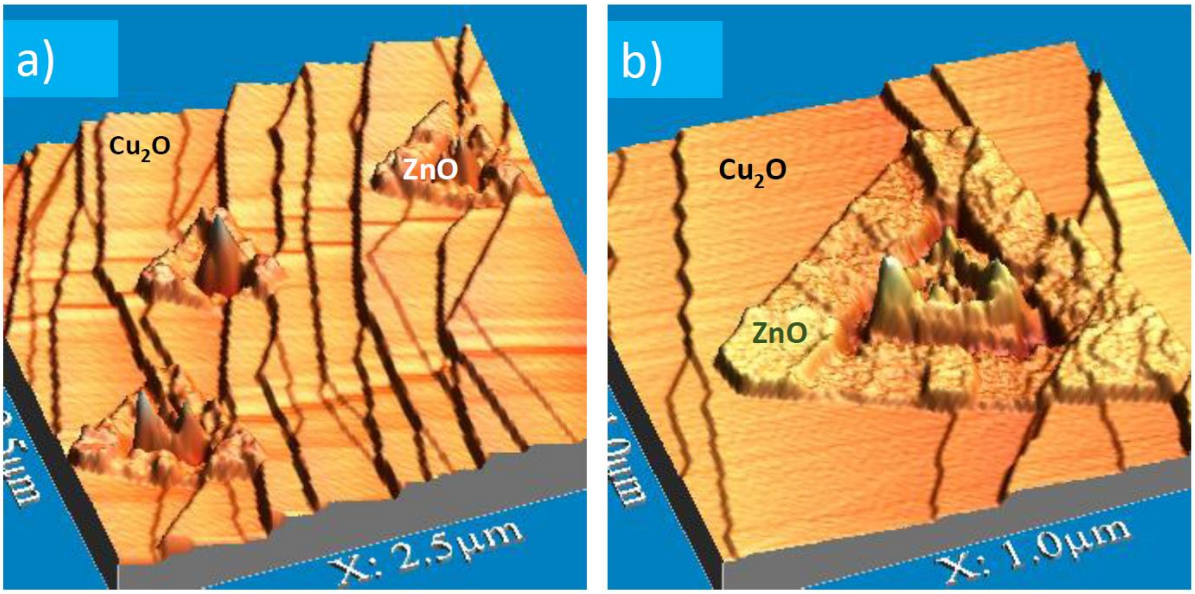

Figure 1. Three-Dimensional (3D) view of ZnO islands deposited on a Cu_xO/Cu(111) substrate. The scale is 2500 nm^2 on the left (a) and 1000 nm^2 on the right (b). The images were collected using a tunneling current I_t= 0.13 nA and a sample bias V_{tip} = 1.3 V.

2. Results and discussion:

2.1 Methane activation and production of methanol on $ZnO/Cu_2O/Cu(111)$ surfaces under CH_4/O_2 mixtures.

2.1.1 Catalytic studies

In the first set of experiments, we investigated the conversion of CH_4 to CH_3OH on $ZnO/Cu_2O/Cu(111)$ surfaces using a reaction mixture of CH_4/O_2 in a batch reactor. The products of the reaction were CO, CO_2, H_2O, H_2 and CH_3OH. The temperature of the system was maintained at 450 K to avoid the further oxidation of CH_3OH into CO/CO_2. The top panel in Figure 2 shows the evolution of the C-containing products as a function of the content of ZnO in the $ZnO/Cu_2O/Cu(111)$ catalysts. Without the addition of ZnO, the $Cu_2O/Cu(111)$ system was not catalytically active for the conversion of CH_4 to CH_3OH and only produced traces of CO, CO_2, H_2 and H_2O when exposed to a mixture of CH_4/O_2. The addition of ZnO to $Cu_2O/Cu(111)$ led to an increase in the conversion rate of CH_4, and CH_3OH appeared as a significant product. The best catalytic performance was seen when the copper oxide substrate was 30% covered by zinc oxide. In these experiments, post-reaction characterization with XPS indicated that there was not reduction of the zinc or the copper oxides under reaction conditions and the O_2 in the reaction feed was necessary for the steady-state production of CH_3OH, CO, CO_2 and H_2. Methane alone could reduce the copper oxide in the catalysts at 450 K, but its reducing power was lower than the oxidative power of O_2.

In the bottom of Figure 2, the maximum selectivity of the $ZnO/Cu_2O/Cu(111)$ catalyst towards the production of CH_3OH is plotted together with values reported before for $Ni/CeO_2(111)$ and $CeO_2/CuO_x/Cu(111)$ catalysts[19, 34], systems which were also able to transform methane into methanol in the absence of water. The performance of the $ZnO/Cu_2O/Cu(111)$ surfaces is clearly

superior with a selectivity towards methanol production in the range of 23-30%. In order to achieve a comparable selectivity in the case of Ni/CeO_2(111), water must be added to the reaction feed[34].

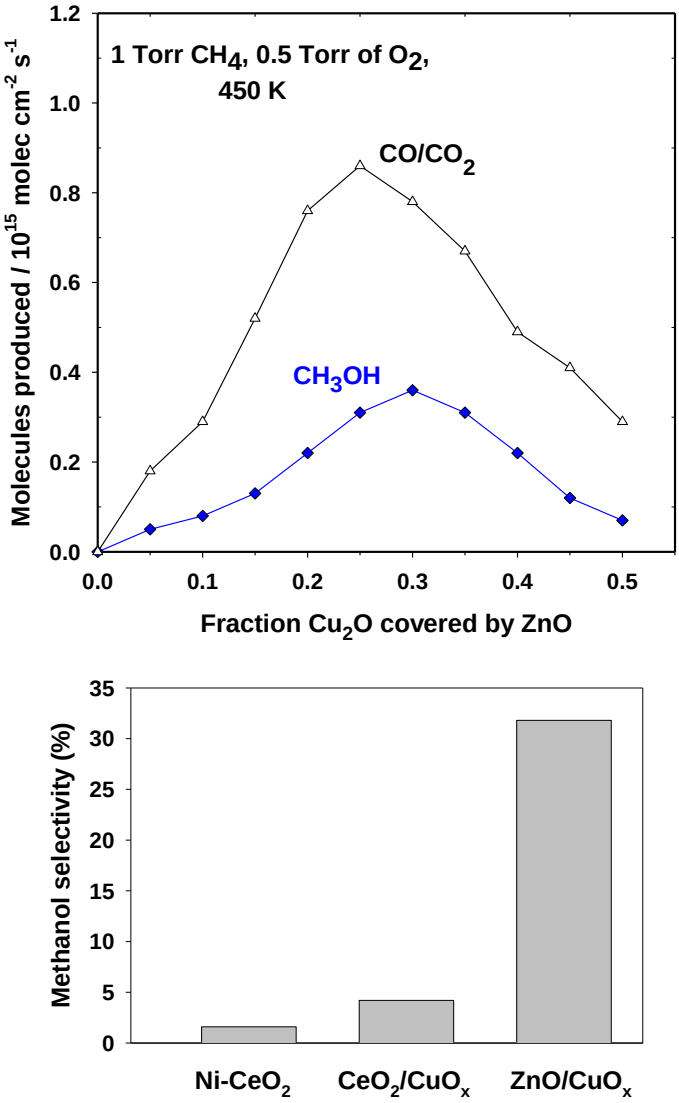

Figure 2. (Top) Variation in the activities of ZnO/Cu_2O/Cu(111) surfaces as a function of ZnO coverage. (Bottom) Comparison of the selectivities for methanol formation of ZnO/CuO_x/Cu(111), CeO_2/CuO_x/Cu(111) {reproduced from Ref. 19. Copyright 2016 American Chemical Society}, Ni/CeO_2(111) {reproduced from Ref. 34. Copyright 2018 American Chemical Society}. All the

experiments were done in a batch reactor at 450 K with pressures of 1 Torr of CH_4 and 0.5 Torr of O_2.

2.1.2 AP-XPS studies

First, it is important to establish the reactivity of $ZnO/Cu_2O/Cu(111)$ towards methane. Figure 3 displays C 1s XPS spectra acquired while exposing a $ZnO/Cu_2O/Cu(111)$ surface to different pressures of methane at 300 K. Methane exposure leads to three observable peaks at 284.4 eV, 286.3 eV, and 288.3 eV that increase in concentration with pressure. Methane undergoes dissociative adsorption ($*CH_4 \rightarrow *CH_x + (4\text{-}x)\ *H$) at room temperature, as evidenced by the CH_x features present at a binding energy of 284.4 eV.[18, 34] Adsorbed *H species are likely stabilized on

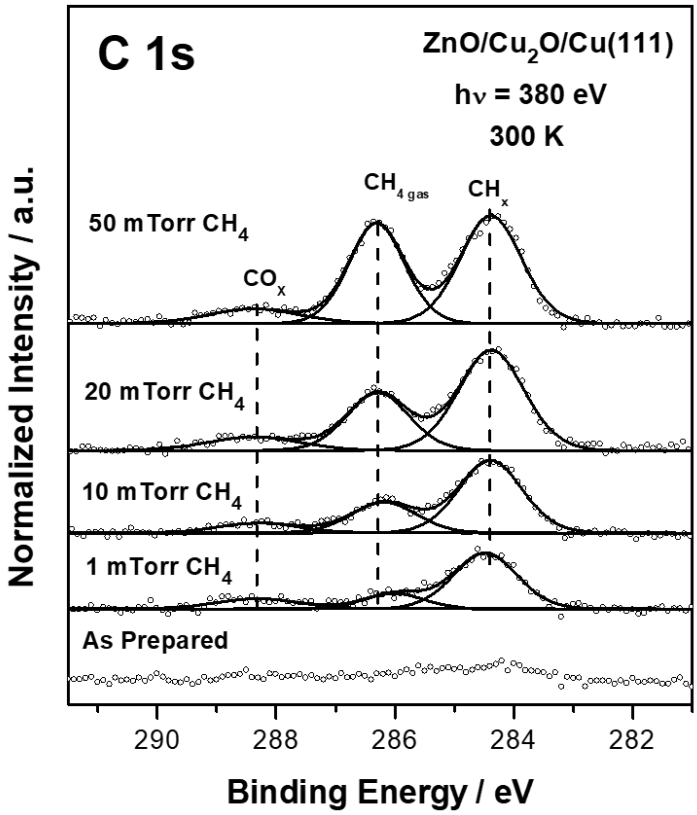

Figure 3: A $ZnO/Cu_2O/Cu(111)$ surface exposed to methane at room temperature (300 K). The evolution of the CH_x peak is shown under increasing methane pressure. Approximately one third of the copper oxide surface was covered by zinc oxide.

the surface in the form of OH, as shown in the corresponding O 1s spectra (Figure S1). Increasing the pressure from 1 to 10, 20, and 50 mTorr allows for a clear distinction between the bound hydrocarbon products and the spectral fingerprint for CH_4 gas, assigned here to the peak at 286.3 eV.

In Figure 3, a peak at 288.4 eV, labeled as CO_x, is most probably coming from the reaction of oxygen from the surface and C atoms produced by the complete dissociation of methane ($*CH_4 \rightarrow *C + 4*H$). This feature is smaller than the corresponding features observed in AP-XPS after exposing $Ni/CeO_2(111)$ and $CeO_2/Cu_2O/Cu(111)$ to methane[18, 34]. This indicates that the $ZnO/Cu_2O/Cu(111)$ system is not very aggressive for the full decomposition of hydrocarbon fragments and helps to explain the substantial selectivity towards methanol formation seen in Figure 2. The intensity of the CO_x peak increased when the $ZnO/Cu_2O/Cu(111)$ surface was exposed to a mixture of CH_4/O_2, Figure 4a.

The addition of O_2 to CH_4 led to distinct changes in the species present on the surface as seen by AP-XPS. Beginning at 300 K and under an atmosphere of 10 mTorr O_2 and 20 mTorr CH_4, i.e., a stoichiometric ratio for the $CH_4 + \frac{1}{2}O_2 \rightarrow CH_3OH$ reaction, the associated surface chemistry is distinct from that of pure CH_4 in that there are now oxidation products on the surface (Figure 4b). Upon deconvolution, a feature is seen near 285.4 eV which likely comes from CH_3O bound to copper oxide.[35] CH_3O groups bound to ZnO are expected at 286.3 eV,[35, 36] and the feature will overlap with the peak for CH_4 gas. The existence of CH_3O in Figure 4b is consistent with the

production of CH_3OH on $ZnO/Cu_2O/Cu(111)$ after exposing the surface to a CH_4/O_2 mixture (Figure 2). In accordance with the DFT results to be described below, O-O bond cleavage can readily occur on this surface and further oxidize CH_4 or other carbon products present; this is the direct oxidation pathway for CH_3OH production on Zn-O-Cu.

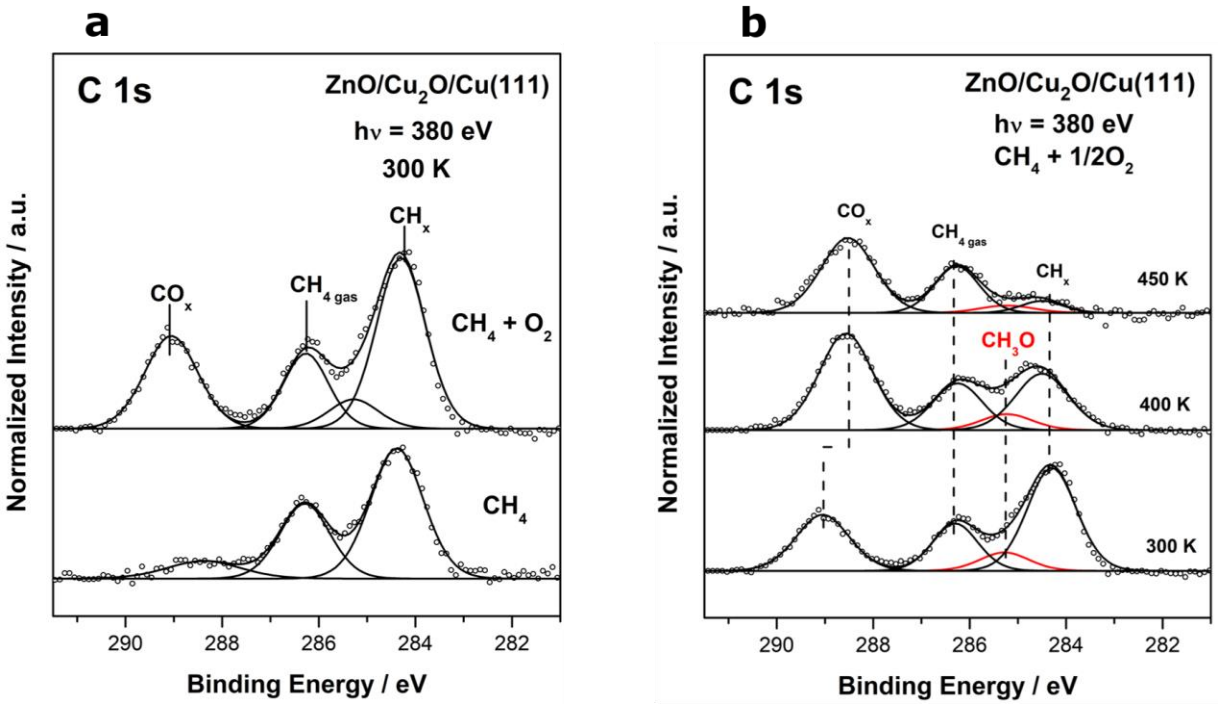

Figure 4. (a) C 1s XPS spectra collected while exposing a $ZnO/Cu_2O/Cu(111)$ surface at 300 K to 20 mTorr of CH_4 (bottom) and 20 mTorr of CH_4 plus 10 mTorr of O_2 (top). (b) $ZnO/Cu_2O/Cu(111)$ exposed to a gas mixture of 20 mTorr CH_4 and 10 mTorr O_2 at 300, 400, and 450 K. Open circles represent the raw data points and the solid black lines are the fitted peaks and their sum. The red peak in (b) is assigned to CH_3O. Approximately one third of the copper oxide surface was covered by zinc oxide.

2.1.3 DFT and KMC studies

To gain a better understanding of the catalytic behavior of $ZnO/Cu_2O/Cu(111)$, DFT calculations together with KMC simulations were performed. The STM images in Figure 1 show complex structures for the rough ZnO islands dispersed on the $Cu_2O/Cu(111)$ substrate. It was found that the ZnO islands exposed surfaces which were rich in steps and contained either O or Zn vacancies.[31-33] Thus, the systems under study in the catalytic tests and AP-XPS measurements offered different types of adsorption sites for the activation of methane and molecular oxygen. Three different models, including a stoichiometric ZnO flat overlayer, a step-rich Zn_3O_3 cluster, and a defected O-rich ZnO overlayer (Figure S4), were used to describe high-coordinated stoichiometric ZnO sites and low-coordinated edge and defect (Zn vacancy or Zn_v in this case) sites of the rough triangular ZnO nanostructures present at the $ZnO-Cu_2O$ interface (Figure 1 and see SI for more details on the models).

Upon exposure to CH_4, the molecule interacted weakly with the stoichiometric ZnO flat overlayer and the step-rich Zn_3O_3 cluster (adsorption energy, E_{ads} = -0.46 kcal/mol, Figures 5a,S5). The corresponding dissociation was very high in both cases (barrier, E_a, of 35.28, 28.82 kcal/mol). In contrast, the O-rich ZnO overlayer exhibited a strong binding at the low-coordinated O site (E_{ads} = -3.00 kcal/mol, Figure 5b) and exhibited a higher activity toward CH_4 dissociation to $*CH_3$ (E_a = 10.84 kcal/mol), which was comparable to the $CeO_2/Cu_2O/Cu(111)$ system for the first C-H bond scission (E_a = 11.76 kcal/mol)[18]. By comparison, the dissociation to directly produce $*CH_3OH$ and an oxygen vacancy (O_v) (E_a = 18.68 kcal/mol) was less favorable (Figure S6). According to the calculated partial density of states (PDOSs), the presence of a Zn_v in the O-rich ZnO overlayer rendered neighboring low-coordinated oxygen species the higher-lying O 2p states than that of the low-coordinated O at the step-rich Zn_3O_3 cluster and the high-coordinated O at the stoichiometric ZnO flat overlayer, thus contributing to the higher catalytic behaviors toward CH_4

adsorption and dissociation (Figure 5c). The *CH_3 fragment could further dissociate to *CH_2 (E_a = 14.07 kcal/mol) and *CH (E_a = 17.52 kcal/mol, Figures S7,8), together with the formation of H_2O and O_v. Given that, among the three types of sites studied, only the O-rich defect of ZnO is active enough to enable facile CH_4 dissociation to *CH_x at room temperature and is therefore the likely site responsible for CH_4 activation observed in AP-XPS (Figure 3).

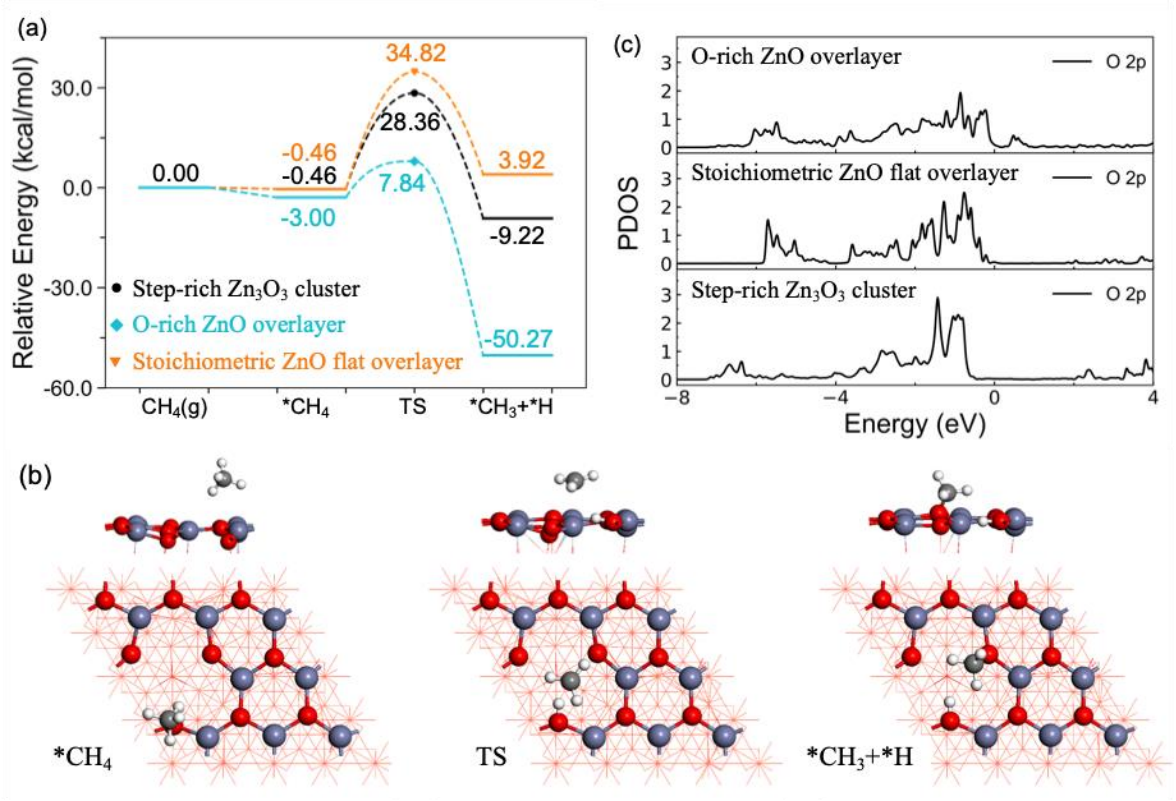

Figure 5: (a) DFT-calculated potential energy diagram for CH_4 dissociation on the stoichiometric ZnO flat overlayer, step-rich Zn_3O_3 cluster and O-rich ZnO overlayer models; (b) Optimized structures of intermediates and transition states (TS) for CH_4 dissociation process on the O-rich ZnO overlayer model; Detailed top and side view structures for all three models were shown in Figure S5. Violet: Zn; brown: Cu; red: O in ZnO/Cu_2O/Cu(111); gray: C; white: H; (c) O 2p partial density of states (PDOS) of for lattice O (the one with dashed circle in Figure S4) associated with

CH_4 dissociation on the stoichiometric ZnO flat overlayer, step-rich Zn_3O_3 cluster and O-rich ZnO overlayer models.

Upon exposure of both CH_4 and O_2, the two gases could compete for active sites. Here, for each intermediate, the multiple competing steps for the sequential reaction were included in the DFT calculations and KMC simulation to confirm the operational reaction sequence. However, this was not the case for the stoichiometric and O-rich ZnO overlayers, where O_2 was only weakly bound (E_{ads}= -0.46 kcal/mol) and the dissociation was less favorable than that of CH_4 (Figure S9a,b). Yet, over the O-rich ZnO overlayer, O_2 helped to fill the O_v produced by CH_4 dissociation and enable a highly exothermic combustion to form CO_2 with energy release of -175.72 kcal/mol, with the highest barrier of 17.52 kcal/mol corresponding to $*CH_2$ dehydrogenation (Figures S7,S8). Due to the synergy between low-coordinated Zn sites and Cu sites of Cu_2O at the ZnO-Cu_2O interface, the step-rich Zn_3O_3 cluster displayed a more favorable O_2 adsorption and dissociation at the Zn-Cu bridge (E_{ads}=-5.77 kcal/mol) than the other two systems (E_a=10.61 kcal/mol, Figure S9c). More importantly, the formed low-coordinated O at the step via a bridging Zn-O-Cu motif (Figures 6a,S10) helped in stabilizing $*CH_4$ (E_{ads} = -0.92 kcal/mol) and facilitating conversion to $*CH_3O$ and $*CH_3OH$, where $*CH_3O$ formation is slightly more favorable (E_a =14.07 kcal/mol) than that of $*CH_3OH$ (E_a = 20.29 kcal/mol). Once $*CH_3O$ was formed, the subsequent oxidative dehydrogenation to $*CO_2$ via $*CH_2O$, *CHO and *HCOO intermediates was highly exothermic with energy release of 141.13 kcal/mol and the highest barrier of 11.30 kcal/mol corresponding to $*H_2CO$ dehydrogenation (Figure 6a). During this process, O_2 not only generated the active site to oxidize CH_4 to $*CH_3O$, but also stabilized ZnO by rapidly filling the O_v (E_a = 10.38 kcal/mol) induced by the surface-bound *H, a species formed during CH_4 reforming process.

According to the KMC simulations based on the DFT calculated barriers and prefactors (see SI for detail, Figure S11, Tables S1-S6), both O-rich ZnO overlayer and step-rich Zn_3O_3 cluster contributed on exposure to a mixture of CH_4 and O_2 (CH_4: O_2 ratio of 2:1 at 450 K); while the reaction was limited on the stoichiometric ZnO flat overlayer (Figure 6). For O-rich ZnO overlayer, a CH_3OH selectivity of only 0.02% and a production rate of 3.76×10^{13} molec $cm^{-2}s^{-1}$ was observed (Figures 6b,c); the majority of CH_4 underwent complete combustion to CO_2 with selectivity of 99.98% and production rate of 1.62×10^{17} molec $cm^{-2}s^{-1}$ due to the preferential $*CH_4$ dissociation to $*CH_3$ (E_a = 10.84 kcal/mol) over the oxidative dissociation to $*CH_3OH$ (E_a = 18.68

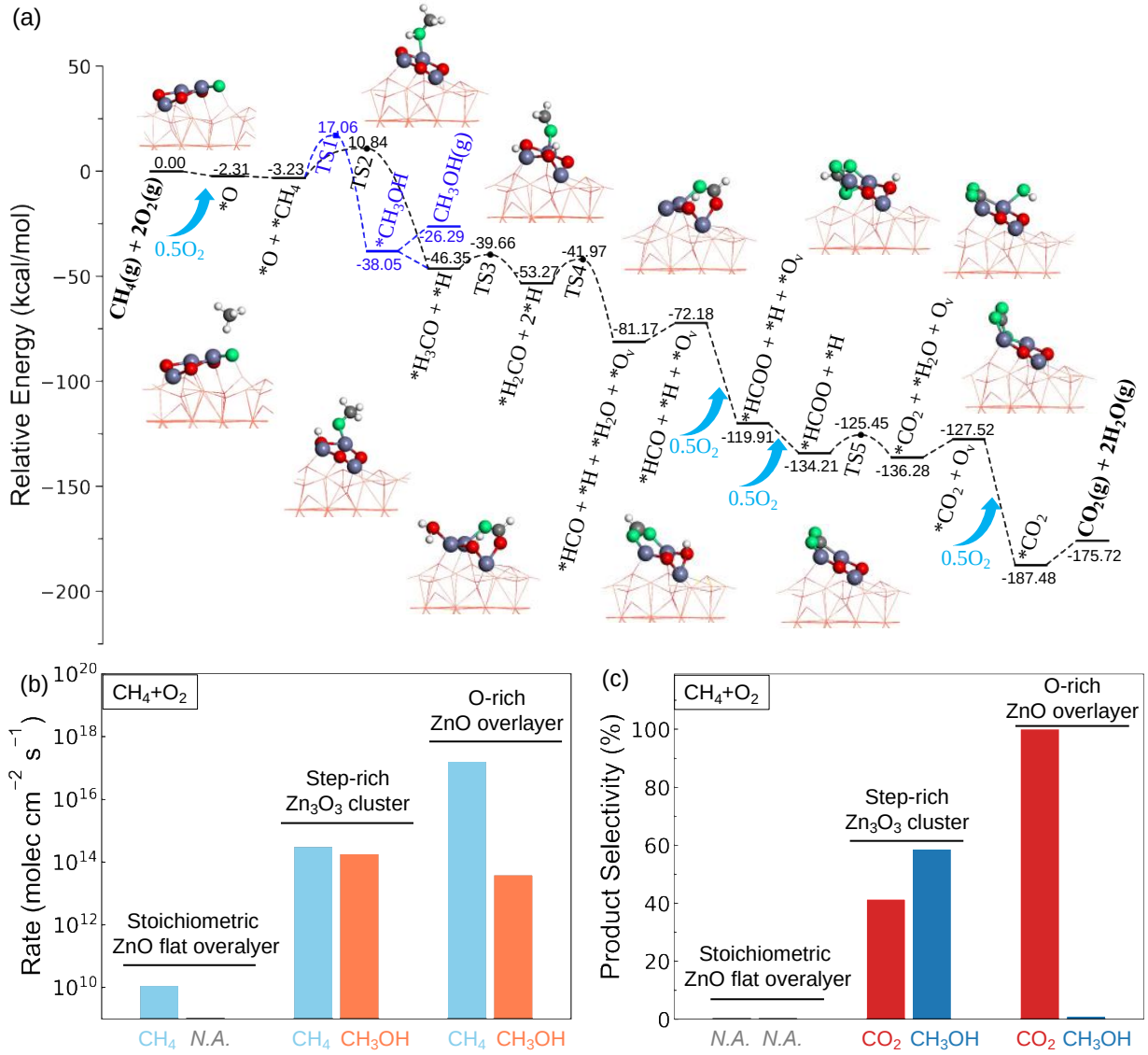

Figure 6 (a) DFT-calculated potential energy diagram for reaction network of CH_4 oxidation by O_2 at ZnO-Cu_2O step of step-rich Zn_3O_3 cluster model. Inset: Structures for selected intermediates, also see Figure S10. Violet: Zn; brown: Cu; red: O in ZnO/Cu_2O/Cu(111); Green: O from O_2; gray: C; white: H. KMC-simulated reaction rates of CH_4 reforming and CH_3OH production (b), products selectivity (c) over stoichiometric ZnO flat overlayer, step-rich Zn_3O_3 cluster and O-rich ZnO overlayer models on exposure to CH_4 and O_2 with a pressure ratio of 2:1at 450 K.

kcal/mol). That is, O-rich ZnO overlayer is too active to enable the mild oxidation of CH_4 to CH_3OH. Upon going to step-rich Zn_3O_3 cluster, an increase in CH_3OH selectivity to 58.74% and production rate of 1.78×10^{14} molec $cm^{-2}s^{-1}$ was achieved (Figures 6b,c). At steady states during KMC simulations, only small amount of $*CH_x$ and *OH was observed on O-rich ZnO overlayer (Figures S12a,b), in accordance with experimental observations by AP-XPS (Figure 4).

Therefore, the combined DFT and KMC simulations revealed that upon exposure to CH_4 and O_2 the CH_3OH selectivity and production on $ZnO/Cu_2O/Cu(111)$ strongly depended on the local structure of ZnO sites. Under a mixture of CH_4 : O_2 at a ratio of 2:1 at 450K, the step-rich Zn_3O_3 cluster sites dominated the CH_3OH production, which was about ten times higher than that of the O-rich ZnO overlayer sites. CO_2 was the major product which originated mainly from the defect O-rich ZnO sites. While the stoichiometric ZnO flat overlayer sites barely produced the CH_3OH products.

The observed enhancement of CH_3OH selectivity at the step-rich Zn_3O_3 cluster site was not seen on the step-rich Ce_3O_6 cluster site on the $CeO_2/Cu_2O/Cu(111)$ system[18], which only exhibited a CH_3OH selectivity less than 0.1 % and CH_3OH production rate of 1.40×10^{12} molec $cm^{-2}s^{-1}$ under the same conditions (Figure 7). This could be ascribed to the weakened binding of CH_3OH (E_{ads} = -11.76 kcal/mol) as compared to $CeO_2/Cu_2O/Cu(111)$ (E_{ads} = -20.06 kcal/mol)[18]. As a result, the desorption of as-formed $*CH_3OH$ species at $ZnO\text{-}Cu_2O$ step site was facilitated and able to compete with the dissociation process to $*CH_3O$ + *H, that led to a full combustion to CO_2 (Figure 6a). In addition, the recombination of $*CH_3O$ and surface *H species to $*CH_3OH$ was also competitive (E_a = 8.30 kcal/mol) at the $ZnO\text{-}Cu_2O$ step with the dissociation of $*CH_3O$ to $*CH_2O$ (E_a = 6.69 kcal/mol), which enabled the high production of CH_3OH. This was demonstrated by the observed soaring operation times for forward and reverse reaction, $*CH_3OH \leftrightarrow *CH_3O$ + *H,

during KMC simulations, a phenomenon that was not presented by the $CeO_2/Cu_2O/Cu(111)$ system due to the faster $*CH_3O$ to $*CH_2O$ conversion process (E_a = 7.15 kcal/mol) with an eventually full combustion and slower $*CH_3O$ recombination with surface *H to $*CH_3OH$ (E_a = 14.53 kcal/mol)[18].

Overall, multiple factors contributed to the observed high CH_3OH product selectivity and rate on $ZnO/Cu_2O/Cu(111)$ by reforming CH_4 under the O_2 environment. First, an active center (in this case, bridging Zn-O-Cu motif at step-rich Zn_3O_3 cluster) should be formed to address the well-known critical step that directly activates CH_4 to $*CH_3OH$. Second, with the formation of $*CH_3OH$ species, the subsequent desorption of $*CH_3OH$ should not be an obstacle. Third, a faster recombination of $*CH_3O$ and *H species and a slower $*CH_3O$ decomposition serves as another key factor for achieving high CH_3OH selectivity.

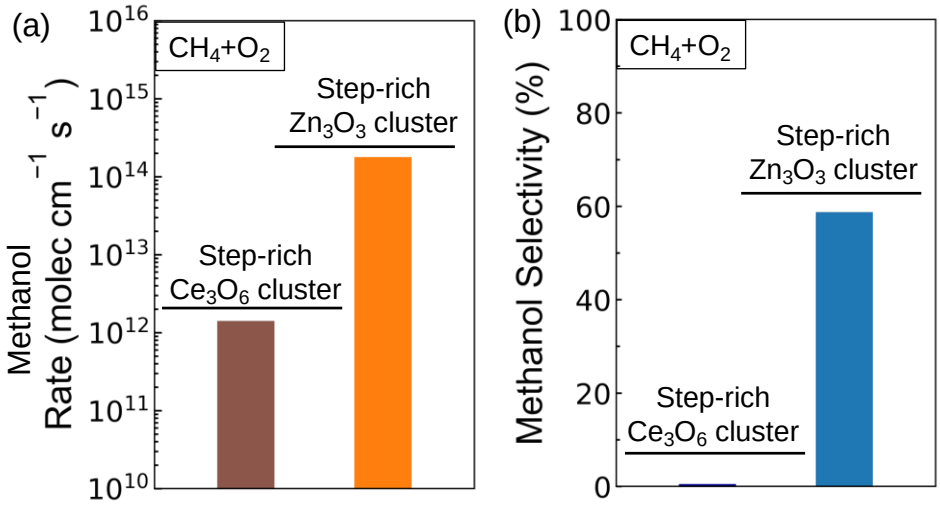

Figure 7: Comparison of KMC-simulated CH_3OH production rate (a) and selectivity (b) on step-rich Zn_3O_3 cluster and step-rich Ce_3O_6 cluster supported by $Cu_2O/Cu(111)$ surface on exposure to CH_4 and O_2 mixture with a pressure ratio of 2:1 at 450K.

2.2 Methane activation and production of methanol on $ZnO/Cu_2O/Cu(111)$ surfaces under $CH_4/O_2/H_2O$ mixtures.

2.2.1 Catalytic studies

Water plays an essential role in the conversion of methane to methanol on Cu-exchanged zeolites[15-17]. A minor amount of water (< 0.1 Torr) was formed during the experiments of Figure 2. This small amount of water is not able to switch the selectivity towards methanol formation (Figure S13). However, we found that the addition of large amounts of water (2-4 Torr, Figure S13) to the CH_4/O_2 reaction feed substantially enhanced the selectivity towards methanol production (Figure 8). Under a $CH_4/O_2/H_2O$ reaction mixture (Figure 8a), a $Cu_2O/Cu(111)$ surface covered ~ 25% by ZnO displays a selectivity of 84% for CH_3OH production, a selectivity which is much greater than those reported for other heterogeneous catalysts under similar reaction conditions[15-18, 34]. The large H_2O/CH_4 ratio that is necessary to induce the shift in selectivity towards methanol production suggests that a new surface configuration determined by hydroxylation or a different reaction path involving OH groups are responsible for the generation of the alcohol in the presence of water. These two possibilities will be examined below using AP-XPS, DFT calculations and KMC simulations.

In Figure 8b, there is a strong effect of the ZnO coverage on the catalytic activity of the $ZnO/Cu_2O/Cu(111)$ surfaces. For surfaces with a ZnO coverage above 35%, there is a substantial drop in the production of methanol. This trend of decreasing activity was also seen when working with a CH_4/O_2 reaction feed (Figure 2). For the large coverages of ZnO, STM images showed the formation of large islands of the oxide overlayer with a decrease in the fraction of the area occupied by the $ZnO\text{-}Cu_2O$ interface[31], where the $CH_4 \rightarrow CH_3OH$ conversion likely takes place.

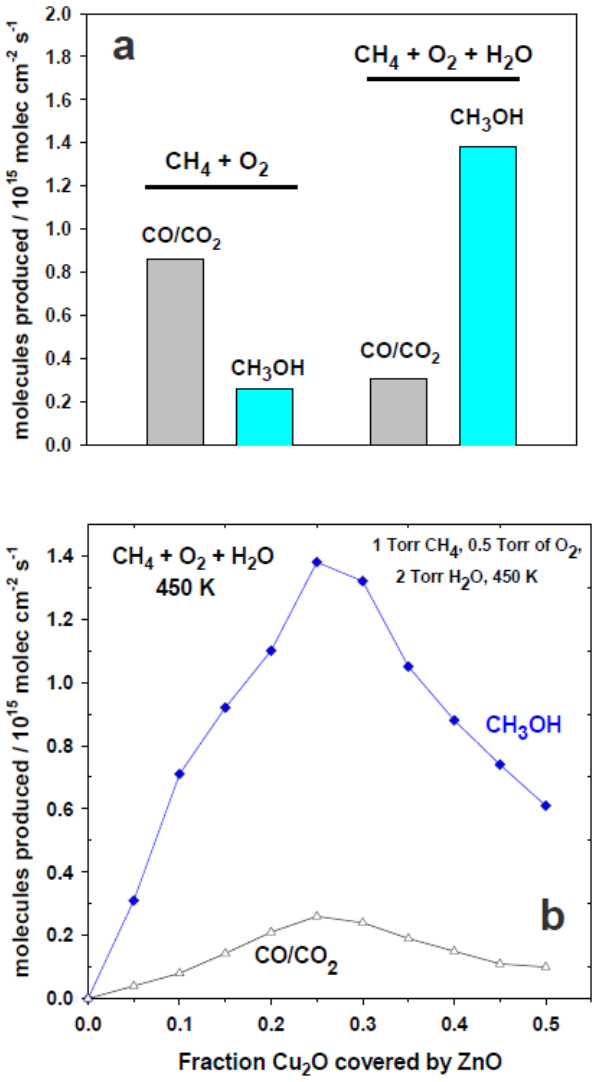

Figure 8. (a) Activities of a ZnO/Cu_2O/Cu(111) surface exposed to reaction mixtures of CH_4/O_2 and $CH_4/O_2/H_2O$. 25% of the copper oxide was covered by ZnO. (b) Variation in the activities of ZnO/Cu_2O/Cu(111) surfaces as a function of ZnO coverage. All the experiments were done in a batch reactor at 450 K with pressures of 1 Torr of CH_4 and 0.5 Torr of O_2. In the case of $CH_4/O_2/H_2O$ reaction mixtures, 2 Torr of H_2O were added.

2.2.2 AP-XPS studies

The results of AP-XPS show a distinct chemistry when a $ZnO/Cu_2O/Cu(111)$ surface is exposed to a mixture of $CH_4/O_2/H_2O$ at 300 K, Figure 9a. At room temperature, we detected that water enhances the amount of CH_x (B.E 284.4 - 284.5 eV) present by a factor of 1.5. A comparison between the reaction mixtures with and without the addition of water ("wet" and "dry" conditions, respectively) are shown in Figure S2 where the difference in adsorbed species is further discussed. There are also clear peaks for CO_x and CH_3O species. In Figure 9b, in contrast to the dry reaction mixture (Figure 4b), heating under a $CH_4/O_2/H_2O$ environment to 400 K induced a growth of the CH_3O peak, which is now well defined and present at 285.3 eV. Zn-bound CH_3O exhibits a higher energy than Cu-bound methoxy, appearing at 286.3 eV[35, 36] under the CH_4 gas peak. AP-XPS experiments with ZnO/Cu_2O under CH_3OH gas have shown that CH_3O binds to both Cu and Zn sites[35]. According to the DFT calculations, the bindings of CH_3O on $Cu_2O/Cu(111)$ (-29.98 kcal/mol) and the step-rich Zn_3O_3 cluster (-33.90 kcal/mol) are stronger than on overlayers of stoichiometric ZnO (-20.75 kcal/mol) and the O-rich ZnO (-11.99 kcal/mol). The mobility of the adsorbed CH_3O species can be high under a reaction temperature of 450 K, going from the O-rich ZnO overlayer to the step-rich Zn_3O_3 cluster site for further combustion to CO_2 or hydrogenation to $*CH_3OH$, which were found as fairly facile steps with relatively low barriers (< 12.5 kcal/mol, Figure 6a, Tables S1 and S5). Alternatively, the adsorbed $*CH_3O$ can diffuse to the stoichiometric ZnO flat overlayer or to the Cu_2O layer as observed experimentally (Figure 9), which is less favorable than to the step-rich Zn_3O_3 cluster sites. However, the ZnO flat overlayer and Cu_2O layer were found to be inactive for the reaction. When going from a reaction feed of CH_4/O_2 (Figure 4b) to $CH_4/O_2/H_2O$ (Figure 9b), the enhancement in the concentration of CH_3O on the catalyst surface is clear at 400 and 450 K.

At a reaction temperature of 450 K, the contrast between the wet and dry reaction is most pronounced; while the dry reaction mixture contains very little besides CO_x products, the wet reaction has additional surface intermediates of CH_3O, CH_x, and surface carbon. A comparison of the CH_3O peak area in these two reaction mixtures at 450 K is displayed in Figure S3, which shows an increase by a factor ~10.

The relative amounts of CH_3O seen in the AP-XPS data of Figure 9 are consistent with the kinetic results in Figure 8 where the addition of water to the reaction feed enhances the conversion of CH_4 and substantially improves the selectivity towards CH_3OH production. As we will see below, the photoemission results also agree with results of KMC simulations in which adsorbed OH groups facilitate CH_4 dissociation, participate in the formation of CH_3O, and help in its desorption from the catalyst surface.

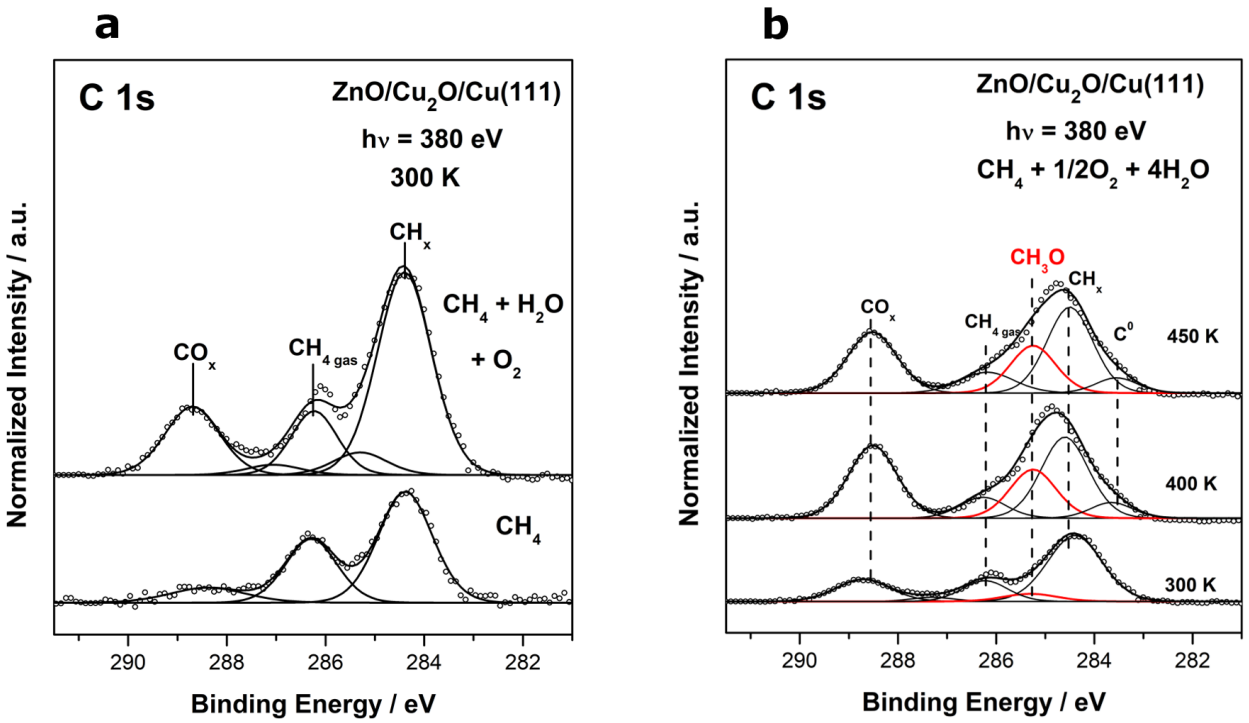

Figure 9. (a) C 1s XPS spectra collected while exposing a $ZnO/Cu_2O/Cu(111)$ surface at 300 K to 20 mTorr of CH_4 (bottom) and 20 mTorr of CH_4 plus 10 mTorr of O_2 and 80 mTorr of H_2O

(top). (b) $ZnO/Cu_2O/Cu(111)$ exposed to a gas mixture of 80 mTorr H_2O, 20 mTorr CH_4 and 10 mTorr O_2 at 300, 400, and 450 K. Open circles represent the raw data points and the solid black lines are the fitted peaks and their sum. The red peak in (b) is assigned to CH_3O. Approximately one third of the copper oxide surface was covered by zinc oxide.

The DFT results described below show a water-mediated CH_3O extraction pathway. This extraction mechanism was explored in a set of AP-XPS experiments. In a sequence of experiments, 10 mTorr of CH_3OH gas was exposed to two different coverages of $ZnO/Cu_2O/Cu(111)$ (θ = 0.2 ML and 0.4 ML), producing CH_3O fragments bound to the surface that remained adsorbed upon evacuation of the CH_3OH gas, see Figure 10. It is clear that on the $ZnO/Cu_2O/Cu(111)$ surfaces the fraction of CH_3O groups that undergo full decomposition to yield C and CO_x species is minor. Secondary products of the adsorption of CH_3OH are C (284.4 eV), CO or H_2CO (287.8 eV), and CO_2 or CO_3 (289.3 eV)[35]. We explored how difficult it is to remove the adsorbed CH_3O groups. Onto these methanol exposed systems, a small amount of water (2×10^{-6} Torr) was dosed at room temperature. It induced a desorption of most of the CH_3O bound to ZnO and Cu_2O sites. Thus, the XPS results in Figures 9 and 10 indicate that water facilitates both the formation and extraction of CH_3O from the $ZnO/Cu_2O/Cu(111)$ catalyst. This helps to explain the improvement in CH_3OH selectivity seen in Figure 8.

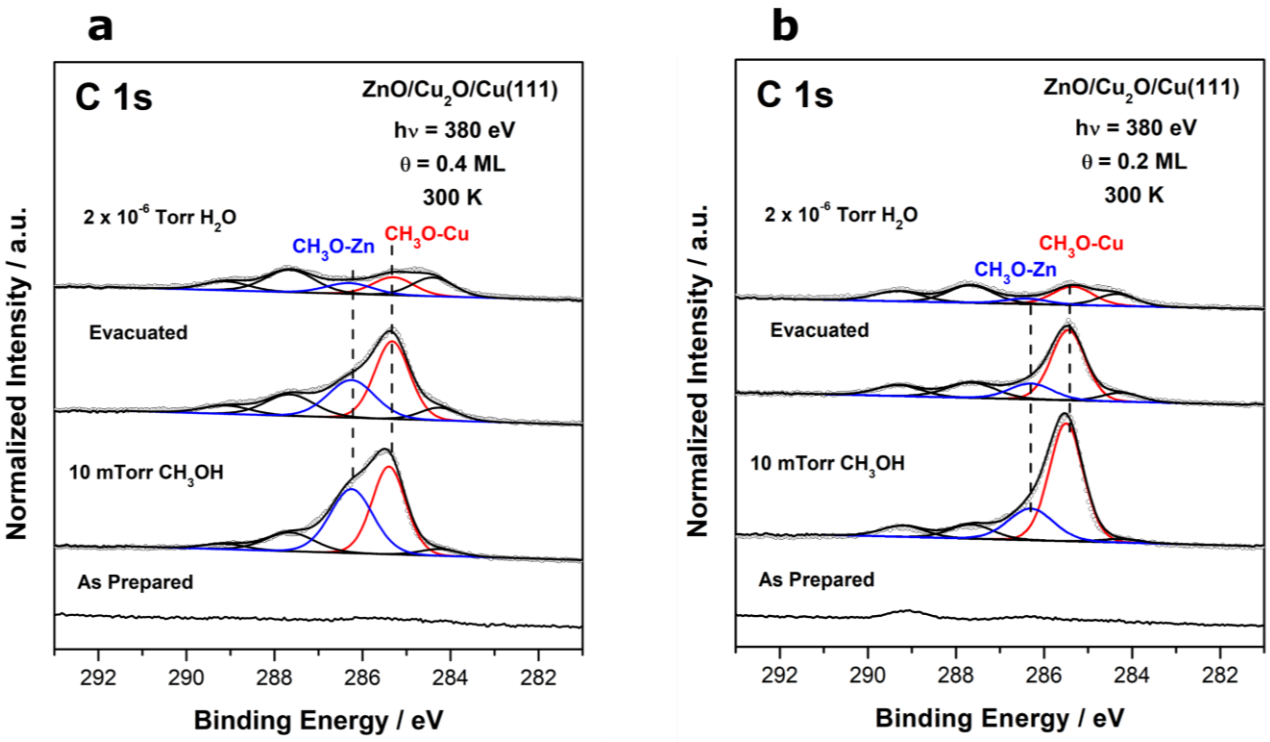

Figure 10. $ZnO/Cu_2O/Cu(111)$ surfaces exposed to 10 mTorr of methanol followed by evacuation and exposure to 2 x 10^{-6} Torr H_2O. The ZnO coverages are 0.2 ML (left, a) and 0.4 ML (right, b). The Zn-bound methoxy (blue) and Cu-bound methoxy (red) are labeled for clarity

2.2.3 DFT and KMC studies

Our DFT calculations showed that the addition of H_2O to CH_4 and O_2 altered the reaction network significantly due to the preferential dissociative adsorption of H_2O over CH_4 and O_2 on all three models (Figure S9). It resulted in the formation of *OH species at the Zn site, which hindered the O_2/CH_4 dissociation. More importantly, *OH (bound to Zn) acted as the new active site. Specifically, the *OH species at O-rich ZnO overlayer was the most active to enable the direct

CH_4 to CH_3OH reforming (E_a = 16.60 kcal/mol) due to the higher-lying O 2p states of *OH species than those top *OH species at step-rich Zn_3O_3 cluster and stoichiometric ZnO flat overlayer (Figures 11,S14,S15).

The formed *CH_3OH could undergo either a direct desorption (E_a = 6.00 kcal/mol) or dissociation to *CH_3O species (E_a = 2.08 kcal/mol). Consistent with AP-XPS results (Figure 10), the DFT calculations showed that the facile extraction of *CH_3O by H_2O, due to the preferential *CH_3O···HOH interaction via hydrogen bonding. It produced *CH_3OH at the binding site (E_a = 11.99 kcal/mol, Figures 11,S16), which was replaced by *OH sequentially and released to gas phase as a product (E_a= 9.46 kcal/mol). Furthermore, H_2O also helped with the removal of surface -bound *H species in the form H_2O by forming a *HOH···OH structure via hydrogen bonds (Figures 11a,S15). In addition, the presence of O_2 was necessary to assure the stability of ZnO nanostructures under reaction conditions by filling O_v generated during the *H removal. By comparison, higher activation energies for *OH-activated CH_4→CH_3OH reforming were required

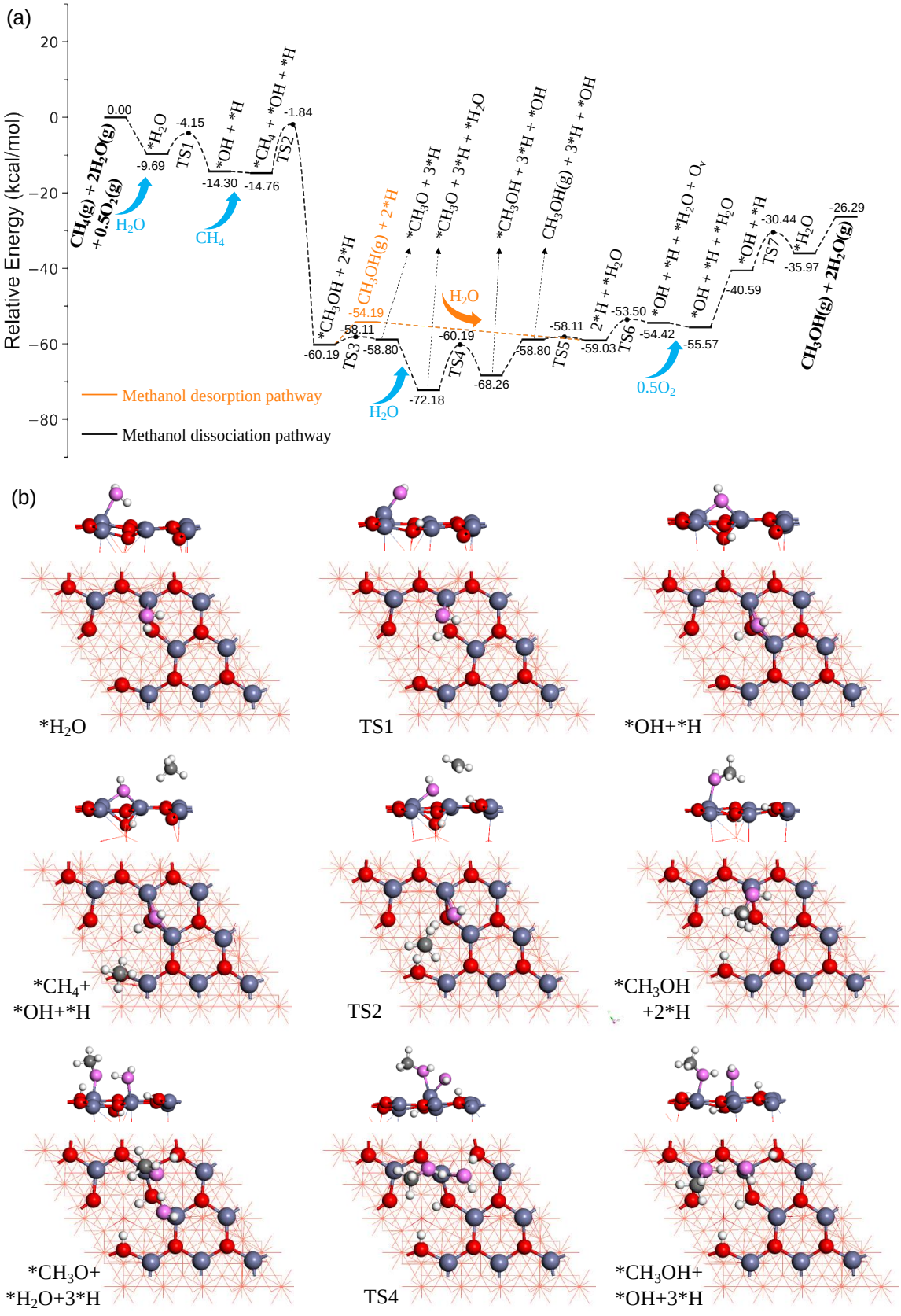
(a)
Relative Energy (kcal/mol)
20
0
−20
−40
−60
−80
0.00
-9.69
-4.15
-14.30
-14.76
-1.84
-60.19
-58.11
-54.19
-58.80
-72.18
-60.19
-68.26
-58.80
-58.11
-59.03
-53.50
-54.42
-55.57
-40.59
-30.44
-35.97
-26.29
CH4(g) + 2H2O(g) + 0.5O2(g)
*H2O
TS1
*OH + *H
*CH4 + *OH + *H
TS2
*CH3OH + 2*H
CH3OH(g) + 2*H
TS3
*CH3O + 3*H
*CH3O + 3*H + *H2O
TS4
*CH3OH + 3*H + *OH
CH3OH(g) + 3*H + *OH
TS5
2*H + *H2O
TS6
*OH + *H + *H2O + Ov
*OH + *H + *H2O
*OH + *H
TS7
*H2O
CH3OH(g) + 2H2O(g)
H2O
CH4
H2O
H2O
0.5O2
Methanol desorption pathway
Methanol dissociation pathway
(b)
*H2O
TS1
*OH+*H
*CH4+
*OH+*H
TS2
*CH3OH
+2*H
*CH3O+
*H2O+3*H
TS4
*CH3OH+
*OH+3*H

Figure 11: (a) DFT-calculated potential energy diagram for reaction networks of CH_4 oxidation by O_2 + H_2O at defect site of O-rich ZnO overlayer. (b) Top and side views for selected intermediates and transition states (TS) (also see Figures S15). Violet: Zn; brown: Cu; red: O in $ZnO/Cu_2O/Cu(111)$; Purple: O from H_2O; gray: C; white: H.

to overcome (E_a = 26.06 kcal/mol, 28.13 kcal/mol) on step-rich Zn_3O_3 cluster and stoichiometric ZnO flat overlayer (Figures S17-S20), though a similar pathway was adopted.

Under the KMC-simulated steady state reaction with a mixture of CH_4 : O_2 : H_2O at a ratio of 2:1:8, respectively, and 450K, a similar situation as in the case without H_2O was observed, where the step-rich Zn_3O_3 cluster sites showed a CH_3OH production rate (~2.75×10^{15} molec cm^{-2} s^{-1}) about two orders of magnitude lower than on the O-rich ZnO overlayer sites (~7.02×10^{17} molec cm^{-2} s^{-1}). The stoichiometric ZnO flat overlayer sites remained inactive for CH_3OH production.

The *OH species at the stoichiometric ZnO flat overlayer surface were barely observed (Figure S21), due to its preferential recombination with *H to form *H_2O (E_a = 2.77 kcal/mol) over the reaction with CH_4 (E_a = 28.13 kcal/mol). The weakly bound *OH species led to low CH_4 conversion rate and no CH_3OH produced (Figure 12a), as seen for the case without H_2O (Figure 6b,c).

On the O-rich ZnO overlayer, instead, the defect sites were steadily occupied by *OH (Figure S21) due to the addition of H_2O, enabling a significant increase in CH_4 reforming rate (8.05×10^{17} molec cm^{-2} s^{-1}), CH_3OH selectivity (87.50%), and CH_3OH production rate (7.02×10^{17} molec cm^{-2} s^{-1}) (Figures 12a,b). Such an enhancement strongly depended on the presence of H_2O, via providing enough active *OH species to enable the CH_4 to CH_3OH conversion (Figure 11),

hindering the sites for the direct CH_4 dissociation forming CO_2 (Figure S7) and promoting extraction of $*CH_3O$ in the form of CH_3OH products (Figure S16).

The H_2O-promoted CH_4 reforming rate (2.76×10^{15} molec cm^{-2} s^{-1}), CH_3OH selectivity (99.98%) and CH_3OH production rate (2.75×10^{15} molec cm^{-2} s^{-1}) were also observed on step-rich Zn_3O_3 cluster surfaces (Figures 12a,b). Wherein, the CH_3OH selectivity was the highest among the three systems studied, due to the barrierless dissociative H_2O adsorption which blocked the active Zn-Cu bridge at the step, preventing O_2 dissociation and thus production of CO_2 (Figure 6a). While the rates of CH_4 reforming and CH_3OH production were lower than that of O-rich ZnO overlayer due to its higher barrier for *OH-activated CH_4 to CH_3OH conversion (E_a: 28.13 vs. 16.60 kcal/mol).

At steady state, the accumulation of $*CH_3O$ and *OH were observed (Figure 12c,S21) mainly on the ZnO-Cu_2O step and O-rich ZnO defect sites. Compared to the case without H_2O (Figure S12), the enhanced stability of $*CH_3O$, as observed by AP-XPS (Figure 9b vs 4b), was mainly attributed to the interplay between the negligible-barrier (~ 2 kcal/mol) O-H bond cleavage of $*CH_3OH$ and the facile extraction of $*CH_3O$ by H_2O (~ 12 kcal/mol).

Thus, with addition of H_2O, both the CH_4 conversion rate and CH_3OH selectivity were greatly promoted due to the facile H_2O dissociation and generation of active *OH species to enable direct CH_4 to CH_3OH conversion, a similar process that was also observed on $CeO_2/Cu_2O/Cu(111)$[18]. For the enhanced CH_4 conversion and CH_3OH production rates, the O-rich defect sites outperformed the ZnO-Cu_2O step sites, while the contribution from the stoichiometric ZnO sites was subtle and the ZnO-Cu_2O step sites were more active than the O-rich defect sites in promoting CH_3OH selectivity. Consistent with the experiment shown above, the CH_4 conversion rate at the O-rich ZnO defect sites of $ZnO/Cu_2O/Cu(111)$ was higher than $CeO_2/Cu_2O/Cu(111)$ by a factor

of ~2 according to the KMC results, due to its relative lower barrier in CH_4 oxidation to CH_3OH by *OH (E_a: 16.60 vs. 22.37 kcal/mol). The CH_3OH selectivity at the ZnO-Cu_2O step sites was a slightly higher by a factor of ~1.02 than that of CeO_2/Cu_2O/Cu(111) due to the weaker binding and thus easier *CH_3OH removal (E_{ads}: 11.76 vs. 20.06 kcal/mol). AP-XPS results readily converge with DFT observations at higher temperatures (500 K); Figure S22 compares the wet and dry reaction over ZnO/Cu_2O/Cu(111) at this temperature. Gas phase CH_4 is present in both spectra, but the dry reaction mixture shows virtually no other carbonaceous species. Consistent with DFT results (Figure 6a), the reaction pathway to further oxidation ($CH_4 + 2O_2 \rightarrow CO_2 + 2H_2O$) is complete and no longer solely energetically favorable but also kinetically dominant at 500 K. In comparison, the wet mixture shows a clear peak for CH_3O, the species in the deepest potential energy reaction coordinate in Figure 11 (-72.18 kcal/mol). Note that the relative amount of H_2O present also plays an essential role during the process. Upon exposure to CH_4 and O_2, although H_2O is not added in this case, it is formed during the $CH_4 \rightarrow CH_3OH$ conversion, which is produced due to the reduction of ZnO and accompanied with the formation of O_v on the surface. However, the amount of H_2O produced is much less than the exposed O_2, which acts as the major oxidizing agent for CH_4 conversion according to the DFT and KMC simulation. The addition of H_2O to the mixture of CH_4 and O_2 makes H_2O dissociative adsorption more competitive with respect to O_2 adsorption, and the deposited *OH occupies the active sites and enables the oxidation of CH_4 to *CH_3OH (Figures 11 and S17). In both cases, the presence of O_2 is necessary to fill the O_v and maintain the stability of the catalyst. The overdose of H_2O can hinder the O_2 dissociation at the O_v site and lower the conversion of CH_4, as observed in the catalytic reactor tests (5 Torr in Figure S13).

Overall, due to the formation of unique rough ZnO 2D islands at the ZnO-Cu_2O interface, the catalytic behavior of ZnO/Cu_2O/Cu(111) involved multiple types of sites, which functioned differently depending on the exposed reactive gases. The interplay among these active sites enabled an enhanced CH_4 conversion or CH_3OH selectivity as compared to Ni/CeO_2(111)[34] and CeO_2/Cu_2O/Cu(111)[18, 19]. Particularly, the over-oxidation of formed *CH_3OH to CO_2 can be effectively hindered over the ZnO/Cu_2O/Cu(111) catalyst via different ways to ensure high selectivity to CH_3OH (Figures 6a, 11a, and S17). Upon exposure to CH_4+O_2, the step-rich Zn_3O_3 cluster sites produces *CH_3OH at the Zn site, where the binding is not strong (11.76 kcal/mol), and the desorption instead of further dissociation to *CH_3O and eventually to CO_2 (Figure 6a). With the addition of H_2O, *CH_3OH is formed on both step-rich Zn_3O_3 cluster and O-rich ZnO overlayer sites (Figures 11a and S17). Again, the relatively weak interaction of CH_3OH at the step-rich Zn_3O_3 cluster sites favor the desorption as seen for the case without H_2O. Even if *CH_3OH dissociates, the existence of H_2O in the surroundings populates the surface with a substantial amount of *OH species, which hinder the further decomposition of *CH_3O species. Moreover, H_2O can also hydrogenate *CH_3O to *CH_3OH through a facile extraction process (E_a=12.45 kcal/mol, Figure S17), which is also observed at O-rich ZnO overlayer sites (Figure 11a). With the initial increase of ZnO coverage, the concentrations of both step-rich Zn_3O_3 and O-rich ZnO overlayer sites rises until reaching a maximum at ~ 0.25 ML (Figures 2 and 8). After that point, there is a coalescence of ZnO islands at higher coverages,[31] a phenomenon which removes defects from the oxide overlayer and reduces the concentration of all active sites.

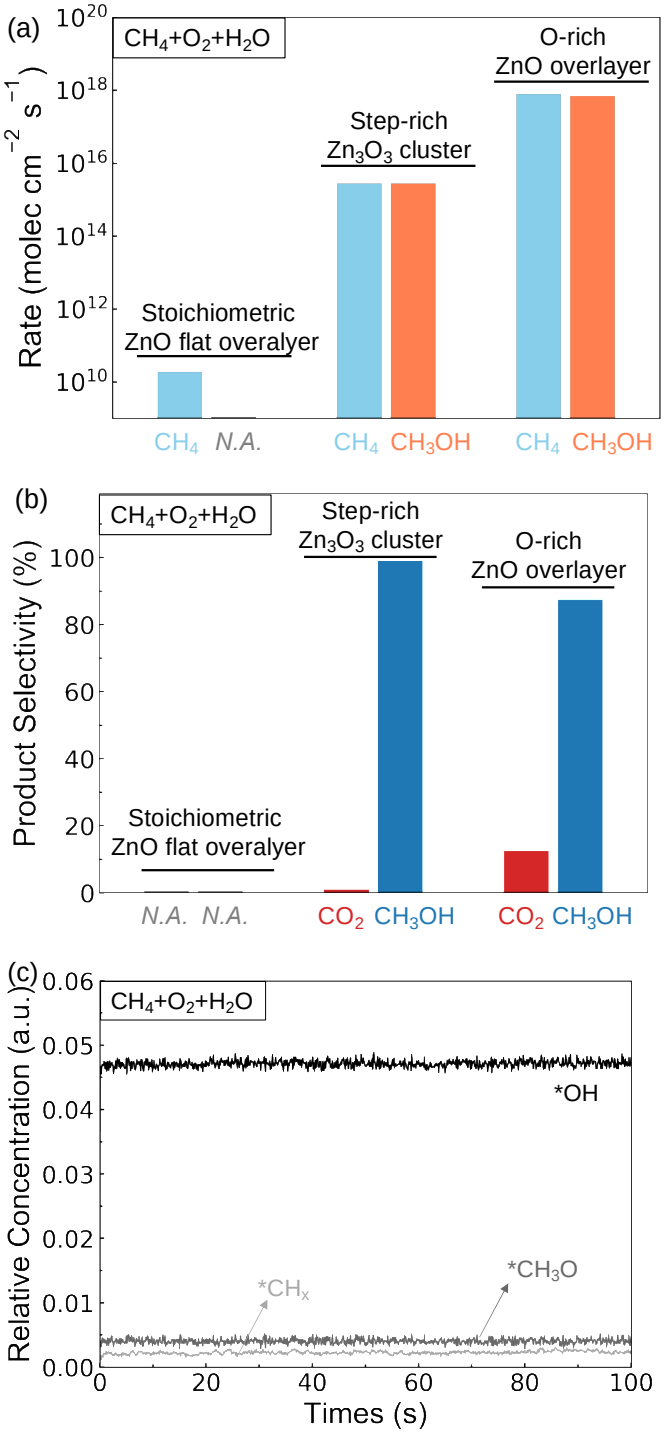

Figure 12: KMC-simulated reaction rates of CH_4 reforming and CH_3OH production (a), product selectivity (b) over stoichiometric ZnO flat overlayer, O-rich ZnO overlayer and step-rich Zn_3O_3

cluster models; (c) Relative concentrations of surface species on $ZnO/Cu_2O/Cu(111)$ catalyst at steady states of on exposure to CH_4, O_2 and H_2O with a gas partial pressure ratio of 2:1:8 at 450K.

3. Conclusions

With a combination of experimental and theoretical studies, it was found that $ZnO/Cu_2O/Cu(111)$ is an active and selective catalysts for the conversion of methane to methanol without water in the feed. The catalyst is multifunctional, thus capable of activating methane at room temperature and transforms methane and oxygen mixtures into methanol at 450 K with a selectivity of ~30%. Upon addition of water, both the methane conversion and methanol selectivity improve, reaching a value higher than 80%. The results of AP-XPS indicate that water facilitates the formation and extraction of CH_3O from the $ZnO/Cu_2O/Cu(111)$ catalyst.

According to the DFT and KMC studies, the superior methane activation and methanol selectivity of $ZnO/Cu_2O/Cu(111)$ are associated with multiple centers, provided by the coarse structures of the supported ZnO islands and strong $ZnO\text{-}Cu_2O$ interactions at the interface, which display different catalytic activity during the reaction. The O-rich defect ZnO sites were identified as the most active for performing the CH_4 conversion on exposure to CH_4, CH_4/O_2 and $CH_4/O_2/H_2O$. Methanol production, instead, was only observed on the $ZnO\text{-}Cu_2O$ step sites upon exposure to CH_4/O_2; while the O-rich defect ZnO sites were found to be too active to enable selective oxidation of methane to methanol and further oxidation to CO_2 was the reaction product for this active site. The addition of water to the CH_4/O_2 mixture greatly enhanced both the methane conversion rate and methanol selectivity due to the facile H_2O dissociation and generation of active *OH species to enable direct CH_4 to CH_3OH conversion. Yet, the O-rich ZnO defect sites showed a more significant promoting effect than the $ZnO\text{-}Cu_2O$ step sites, being able to enable the

methanol selectivity over 80%. Under all three conditions studied the contribution from the stoichiometric ZnO sites remained subtle. Our study points to a new application of the widely used Cu-ZnO catalysts, going beyond conventional CO_2 hydrogenation to a more challenging selective CH_4 to CH_3OH conversion. More importantly, the reported site-dependent behavior opens a new design strategy for guiding selective CH_4 reforming.

4. Experimental and Computational Methods:

4.1 Catalytic tests:

The catalytic activity of the Cu_2O/Cu(111) and ZnO/Cu_2O/Cu(111) surfaces was examined using an instrument which combines an ultrahigh vacuum (UHV) chamber for surface characterization with different techniques (XPS, Auger electron spectroscopy, low-energy electron diffraction, and ion scattering spectroscopy) with a small batch reactor.[18, 19, 27, 30, 31] The Cu_2O/Cu(111) and ZnO/Cu_2O/Cu(111) surfaces were prepared following the methodology described in previous studies.[30, 31] The Cu(111) single crystal (Goodfellow, 99.999%) on which ZnO was deposited was cleaned by successive Ar^+ ion sputtering (1.5 kV, 30 min) and annealing (850 K, 10 min) until deemed sufficiently clean by XPS in the C 1s and O 1s regions. The Zn was vapor-deposited on the Cu(111) crystal at a temperature of 600 K under a O_2 pressure of 5×10^{-7} Torr, resulting in large triangular islands described in detail previously[31] (see Figure 1).

The Cu_2O/Cu(111) and ZnO/Cu_2O/Cu(111) surfaces were introduced in the reactor at 300 K and exposed to reactant feeds of pure CH_4, CH_4/O_2 or $CH_4/O_2/H_2O$. The pressures of methane and O_2 were 1 and 0.5 Torr, respectively, as expected for a stochiometric conversion of methane into methanol (equation 1). The pressure of water was varied in a range from 0 to 4 Torr. For the catalytic tests, the reactor temperature was raised from 300 to 450 K where the measurements were

done. The generation of methanol, CO, CO_2, H_2O and H_2 was followed by a combination of gas chromatography and gas spectroscopy.[18, 19] The kinetic studies were done always under a low conversion of methane (< 5%). Steady-state was reached after 2-3 minutes of reaction and, under the mixtures of CH_4/O_2 or $CH_4/O_2/H_2O$, no signs of catalyst deactivation were found in a period of two hours when the measurements ended.

4.2 Ambient Pressure XPS Experiments:

AP-XPS experiments were performed at beamline 9.3.2 of the Advanced Light Source of Lawrence Berkeley National Laboratory. The binding energy scale was referenced to the Cu 3p core level peak. Photon energies of 380 eV and 650 eV were used to collect the C 1s, Cu 3p, Zn 3p and the O 1s, Cu 3p, and Zn 3p, respectively. A step size of 0.1 eV was used to collect C 1s and O 1s data, resulting in a resolution of ~0.2 eV. XPS data were fitted with a series of Voigt functions with a linear background for C 1s data and Shirley type background for the O 1s data. The fitting was optimized using a least squares fitting optimization. The $ZnO/Cu_2O/Cu(111)$ surfaces were prepared using the methodology described in the previous section which should lead to the morphology seen in Figure 1[31].

4.3 Density Functional Theory (DFT) Calculations:

A spin polarized density functional theory (DFT)[37, 38] implemented in Vienna *ab initio* simulation package (VASP)[39] was used to perform all the calculations. A 400eV kinetic energy

cutoff and the projector augmented wave method (PAW)[40, 41] together with GGA exchange-correlation functional plus the PBE functional[42] were employed. Monkhorst-Pack[43] meshes with 3×3×1 were used to sample the Brillouin zone for all the surface calculations while gamma point were employed for all gas-phase species. The nudged elastic band method (NEB)[44] for each elementary reaction intermediates were performed to derive the transition states. The criteria for total energies and forces on all atoms were set as 10^{-5} eV and 0.02 eV $Å^{-1}$ for convergence, respectively. Gaussian smearing with width 0.05 eV was used to improve the convergence. The Cu (3p, 3d, 4s), Zn (3d, 4s), C (2s, 2p), O (2s, 2p) and H (1s) electrons were treated as valence states, while the remaining electrons were kept frozen as core states. The dispersion forces were not considered here due to the overestimation the strong interactions, e.g., water and oxygen, which represent a major part of the reaction network and thus the activity/selectivity, according to our previous studies[18, 19].

ZnO/Cu_2O/Cu(111) catalyst was simulated with three different models to address the observed rough triangular ZnO nanostructures in STM[29, 31], also shown in Figure 1. One is modeled with 3 layer of 4×4 Cu(111) surface and one monolayer of Cu_xO ($x \approx 1.13$) with Zn_3O_3 cluster for ZnO-Cu_2O step, labeled as step-rich Zn_3O_3 cluster; Another is constructed by one full layer via ZnO$(000\bar{1})$-like motif deposited on top of Cu_2O/Cu(111) for ZnO island terrace, labeled as stoichiometric ZnO flat overlayer; The third model is built by removing one Zn vacancy from the stoichiometric ZnO flat overlayer for ZnO island roughness, labeled as O-rich ZnO overlayer (Figure S4). Note that different from the O-rich defect resulted from Zn vacancy (Zn_v), the Zn-rich defect resulted from O vacancy (O_v) is not stable, where the O_v was likely to be filled under the oxidizing conditions studied here. The Hubbard-like U term[45] was considered to address Cu 3d

electrons for the Cu_xO surface (U_{eff} = 5.2), in which the Coulomb U and exchange J parameters were combined into a single parameter U_{eff} = U - J. During DFT optimizations, bottom two layers were fixed while the rest were allowed to relax with adsorbates. The optimized structure of stoichiometric ZnO flat overlayer showed a non-polar graphite-like structure instead of the polar wurtzite structure, which is in consistent with recent reports that ZnO graphitic structures were observed experimentally or calculated theoretically when only thin layers ($\leqslant$ 4) of ZnO grown on metal supports[23, 46-48].

Overall, the adsorption energy of adsorbate on the ZnO/Cu_2O/Cu(111) model surface was calculated as:

$E_{ads} = E(\text{Adsorbate/Surface}) - E(\text{Surface}) - \text{E(Adsorbate)}$

where E is the total energy obtained from DFT calculations incorporated with zero-point energy (ZPE) correction E_{ZPE}:

$$E_{ZPE} = \sum_{i}^{number\ of\ modes} \frac{1}{2} h\nu_i$$

where ν_i is DFT calculated vibrational frequency by harmonic normal mode approximation for each intermediate.

4.4 Kinetic Monte Carlo (KMC) Simulations:

In KMC simulations, to fully describe the characters of STM observed rough triangular ZnO nanostructures (Figure 1), large ZnO triangle islands were randomly distributed on a Cu_2O layer supported by a 128 × 128 matrix of Cu(111), corresponding to 0.24 monolayer (ML) of coverage with respect to Cu on Cu(111) (Figure S11), which led to the peak rate (Figures 2 and 8). Such KMC matrix enabled a qualitative description of the experimental measurements; yet

quantitative comparisons were very difficult due to the limitation in atomic-level characterization and the high computational cost for modeling the complex catalysts. The step between the ZnO triangle islands and Cu_2O/Cu(111) surface were conducted with the inputs from DFT results on step-rich Zn_3O_3 cluster model; the defect sites on top of ZnO triangle islands were conducted with the inputs from DFT results on O-rich ZnO overlayer; while the rest part of the ZnO triangle islands were considered as stoichiometric ZnO flat overlayer for simulations, as shown in Figure S11.

All elementary steps involved in the KMC simulations were listed in Figures 6a, 11a and S6, S7, S17, S18 and Tables S1, S2, S3, S4, S5 and S6. Pressures in KMC simulations for CH_4, O_2, and H_2O were set as 100 Torr, 50 Torr and 400 Torr, respectively.

The elementary reactions rate constant *k* was calculated by Arrhenius equation given by:

$$k = A_0 * exp\left(-\frac{E_a}{k_B T}\right)$$

in which, E_a is the activation energy with ZPE-correction from DFT calculations for each elementary reaction; k_B is the Boltzmann constant and the T stands for the absolute temperature implemented in KMC simulations. A_0 represents pre-exponential factor, a constant for each elementary reaction which may vary by several orders of magnitude for different elementary reactions[49]. In the present work, A_0 was calculated by[50]:

$$A_0 = \frac{k_B T}{h} exp\left(\frac{\Delta S}{k_B}\right)$$

in which, h is Planck's constant. ΔS is the entropy change from initial state to transition state for each elementary reaction. The entropy (S) for each intermediate was estimated with their corresponding DFT calculated vibrational frequency:

$$S = k_B \sum_{i=1}^{number\ of\ modes} \left\{ \frac{h\nu_i/k_B T}{exp\left(h\nu_i/k_B T\right) - 1} - \ln\left[1 - exp\left(-h\nu_i/k_B T\right)\right] \right\}$$

where v_i is the above DFT obtained vibrational frequency for each intermediate during the vibrational frequency calculations.

The entropy for gas phase molecules involving in the elementary steps was taken from NIST Computational Chemistry Comparison and Benchmark Database (CCCBDB)[51]. The calculated pre-exponential factor for each step was listed in Tables S2, S4 and S6.

Furthermore, the adsorption coefficient for gas phase molecules was calculated as[52]:

$$k_{ads} = \frac{PA_{site}\sigma}{\sqrt{2\pi m k_B T}}$$

where P is the pressure of the adsorption gas, A_{site} is the area of a single site (a Zn-centered triangle with three neighbor-O as vertices), σ is the sticking coefficient, and m is the mass of adsorption gas. The sticking coefficients for CH_4, O_2 and H_2O are all set to 1 in our KMC model, the coverage of adsorbed molecules on the surface, which is catalytically interesting, strongly depends on the desorption rate or the binding energy of each molecule.

The reaction rate was calculated with respect to the area of the Cu(111) substrate via the following equation[53]:

$$Rate = \frac{N}{(Sites\ of\ total\ Cu(111)\ substrate) \times (time\ of\ simulation) \times (A_{Cu})}$$

N is the net operating times for corresponding steps during KMC simulations over different ZnO/Cu_2O/Cu(111) model sites with normalized Zn-site concentration. To make the rates among different sites comparable, N is normalized by the number of Zn involved in each kind of active sites of the ZnO island (i.e., stoichiometric ZnO flat overlayer, O-rich ZnO overlayer, step-rich Zn_3O_3 cluster). A_{Cu} is the area for a single Cu site on the Cu(111) substrate.

The products selectivity was calculated as:

$$Selectivity\ (A) = \frac{Rate(A)}{Rate(P)} \times 100\%$$

Where *Rate (A)* stands for the reaction rate for production A and *Rate (P)* stands for the overall reaction rate for all the productions. Here we note that the differences in catalyst structures studied (Figures 1 and S11) and the systematic errors that existed between measurements and calculations make the quantitative comparison between KMC-estimated rates and the experimentally measured values very difficult. Instead, the difference from one type of site to another can be more reliable, which enables the qualitative comparison in trend with the experiment and is the focus of current study.

Supporting Information

XPS spectra; DFT and KMC models of $ZnO/Cu_2O/Cu(111)$ catalyst; structures of DFT optimized intermediates and transition states; DFT-calculated potential energy diagrams, partial density of states, relative energies and kinetical pre-exponential factors; KMC-simulated species concentrations, reaction rates and product selectivity.

Competing interests

The authors declare no competing interests.

Acknowledgements:

The research carried out at Brookhaven National Laboratory (BNL) was supported by the division of Chemical Science, Geoscience, and Bioscience, Office of Basic Energy Science of the US Department of Energy (DOE) under Contract No. DE-SC0012704. SDS was supported by an Early Career Award by the U.S. Department of Energy. All the calculations in this work were performed using computational resources at Center for Functional Nanomaterials (CFN), and the Scientific Data and Computing Center, a component of the Computational Science Initiative, at BNL under Contract No. DE-SC0012704, at the National Energy Research Scientific Computing Center (NERSC), a DOE Office of Science User Facility, supported by the Office of Science of the DOE under contract DE-AC02-05CH11231 and at Stony Brook University, which was founded by National Science Foundation grant (#1531492). This research used resources of the Advanced Light Source, a U.S. DOE Office of Science User Facility under contract no. DE-AC02-05CH11231.

References:

1. Alvarez-Galvan, M. C.; Mota, N.; Ojeda, M.; Rojas, S.; Navarro, R. M.; Fierro, J. L. G., Direct methane conversion routes to chemicals and fuels. *Catal. Today* **2011,** *171* (1), 15-23.
2. Tang, P.; Zhu, Q.; Wu, Z.; Ma, D., Methane activation: the past and future. *Energy Environ. Sci* **2014,** *7* (8), 2580-2591.
3. Luo, L.; Luo, J.; Li, H.; Ren, F.; Zhang, Y.; Liu, A.; Li, W.-X.; Zeng, J., Water enables mild oxidation of methane to methanol on gold single-atom catalysts. *Nat. Commun.* **2021,** *12* (1), 1218.
4. Liang, Z.; Li, T.; Kim, M.; Asthagiri, A.; Weaver, J. F., Low-temperature activation of methane on the IrO_2(110) surface. *Science* **2017,** *356* (6335), 299-303.
5. Liu, Z.; Grinter, D. C.; Lustemberg, P. G.; Nguyen-Phan, T.-D.; Zhou, Y.; Luo, S.; Waluyo, I.; Crumlin, E. J.; Stacchiola, D. J.; Zhou, J.; Carrasco, J.; Busnengo, H. F.; Ganduglia-Pirovano, M. V.; Senanayake, S. D.; Rodriguez, J. A., Dry Reforming of Methane on a Highly-Active Ni-CeO_2 Catalyst: Effects of Metal-Support Interactions on C−H Bond Breaking. *Angew. Chem. Int. Ed.* **2016,** *55* (26), 7455-7459.
6. Fung, V.; Tao, F.; Jiang, D.-e., Low-temperature activation of methane on doped single atoms: descriptor and prediction. *Phys. Chem. Chem. Phys.* **2018,** *20* (35), 22909-22914.
7. Figueras, M.; Gutiérrez, R. A.; Prats, H.; Viñes, F.; Ramírez, P. J.; Illas, F.; Rodriguez, J. A., Boosting the activity of transition metal carbides towards methane activation by nanostructuring. *Phys. Chem. Chem. Phys.* **2020,** *22* (13), 7110-7118.
8. Senanayake, S. D.; Rodriguez, J. A.; Weaver, J. F., Low temperature activation of methane on metal-oxides and complex interfaces: Insights from surface science. *Acc. Chem. Res.* **2020,** *53* (8), 1488-1497.
9. Basile, A., Methane in the environment: Occurrence, uses and production. *Nova Science Publications Inc: New York*, **2013**, pp. 1-311.
10. Khirsariya, P.; Mewada, R. K., Single step oxidation of methane to methanol–Towards better understanding. *Procedia Eng.* **2013,** *51*, 409-415.
11. Chan, S. I.; Yu, S. S. F., Controlled oxidation of hydrocarbons by the membrane-bound methane monooxygenase: The case for a tricopper cluster. *Acc. Chem. Res.* **2008,** *41* (8), 969-979.
12. Olivos-Suarez, A. I.; Szécsényi, À.; Hensen, E. J. M.; Ruiz-Martinez, J.; Pidko, E. A.; Gascon, J., Strategies for the direct catalytic valorization of methane using heterogeneous catalysis: Challenges and opportunities. *ACS Catal.* **2016,** *6* (5), 2965-2981.
13. Ravi, M.; Ranocchiari, M.; van Bokhoven, J. A., The direct catalytic oxidation of methane to methanol—A critical assessment. *Angew. Chem. Int. Ed.* **2017,** *56* (52), 16464-16483.
14. Wang, V. C. C.; Maji, S.; Chen, P. P. Y.; Lee, H. K.; Yu, S. S. F.; Chan, S. I., Alkane oxidation: Methane monooxygenases, related enzymes, and their biomimetics. *Chem. Rev.* **2017,** *117* (13), 8574-8621.
15. Snyder, B. E. R.; Bols, M. L.; Schoonheydt, R. A.; Sels, B. F.; Solomon, E. I., Iron and copper active sites in zeolites and their correlation to metalloenzymes. *Chem. Rev.* **2018,** *118* (5), 2718-2768.
16. Newton, M. A.; Knorpp, A. J.; Sushkevich, V. L.; Palagin, D.; van Bokhoven, J. A., Active sites and mechanisms in the direct conversion of methane to methanol using Cu in zeolitic hosts: a critical examination. *Chem. Soc. Rev.* **2020,** *49* (5), 1449-1486.

17. Kulkarni, A. R.; Zhao, Z. J.; Siahrostami, S.; Norskov, J. K.; Studt, F., Cation-exchanged zeolites for the selective oxidation of methane to methanol. *Catal. Sci. Technol.* **2018,** *8* (1), 114-123.
18. Liu, Z.; Huang, E.; Orozco, I.; Liao, W.; Palomino, R. M.; Rui, N.; Duchoň, T.; Nemšák, S.; Grinter, D. C.; Mahapatra, M.; Liu, P.; Rodriguez, J. A.; Senanayake, S. D., Water-promoted interfacial pathways in methane oxidation to methanol on a CeO_2-Cu_2O catalyst. *Science* **2020,** *368* (6490), 513-517.
19. Zuo, Z.; Ramírez, P. J.; Senanayake, S. D.; Liu, P.; Rodriguez, J. A., Low-temperature conversion of methane to methanol on CeO_x/Cu_2O catalysts: Water controlled activation of the C–H bond. *J. Am. Chem. Soc.* **2016,** *138* (42), 13810-13813.
20. Álvarez, M.; Marín, P.; Ordóñez, S., Direct oxidation of methane to methanol over Cu-zeolites at mild conditions. *Mol. Catal.* **2020,** *487*, 110886.
21. Grundner, S.; Markovits, M. A.; Li, G.; Tromp, M.; Pidko, E. A.; Hensen, E. J.; Jentys, A.; Sanchez-Sanchez, M.; Lercher, J. A., Single-site trinuclear copper oxygen clusters in mordenite for selective conversion of methane to methanol. *Nat. Commun.* **2015,** *6*, 7546.
22. Liu, P.; Yang, Y. X.; White, M. G., Theoretical perspective of alcohol decomposition and synthesis from CO_2 hydrogenation. *Surf. Sci. Rep.* **2013,** *68* (2), 233-272.
23. Lunkenbein, T.; Schumann, J.; Behrens, M.; Schlögl, R.; Willinger, M. G., Formation of a ZnO overlayer in industrial $Cu/ZnO/Al_2O_3$ catalysts induced by strong metal–support interactions. *Angew. Chem. Int. Ed.* **2015,** *54* (15), 4544-4548.
24. Behrens, M.; Studt, F.; Kasatkin, I.; Kuhl, S.; Havecker, M.; Abild-Pedersen, F.; Zander, S.; Girgsdies, F.; Kurr, P.; Kniep, B. L.; Tovar, M.; Fischer, R. W.; Norskov, J. K.; Schlogl, R., The active site of methanol synthesis over $Cu/ZnO/Al_2O_3$ industrial catalysts. *Science* **2012,** *336* (6083), 893-7.
25. Kuld, S.; Thorhauge, M.; Falsig, H.; Elkjær, C. F.; Helveg, S.; Chorkendorff, I.; Sehested, J., Quantifying the promotion of Cu catalysts by ZnO for methanol synthesis. *Science* **2016,** *352* (6288), 969-974.
26. van den Berg, R.; Prieto, G.; Korpershoek, G.; van der Wal, L. I.; van Bunningen, A. J.; Lægsgaard-Jørgensen, S.; de Jongh, P. E.; de Jong, K. P., Structure sensitivity of Cu and CuZn catalysts relevant to industrial methanol synthesis. *Nat. Commun.* **2016,** *7* (1), 13057.
27. Kattel, S.; Ramírez, P. J.; Chen, J. G.; Rodriguez, J. A.; Liu, P., Active sites for CO2 hydrogenation to methanol on Cu/ZnO catalysts. *Science* **2017,** *355* (6331), 1296-1299.
28. Laudenschleger, D.; Ruland, H.; Muhler, M., Identifying the nature of the active sites in methanol synthesis over $Cu/ZnO/Al_2O_3$ catalysts. *Nat. Commun.* **2020,** *11* (1), 3898.
29. Orozco, I.; Huang, E.; Gutiérrez, R. A.; Liu, Z.; Zhang, F.; Mahapatra, M.; Kang, J.; Kersell, H.; Nemsak, S.; Ramírez, P. J.; Senanayake, S. D.; Liu, P.; Rodriguez, J. A., Hydroxylation of ZnO/Cu(1 1 1) inverse catalysts under ambient water vapor and the water–gas shift reaction. *J. Phys. D: Appl. Phys.* **2019,** *52* (45), 454001.
30. Mahapatra, M.; Gutiérrez, R. A.; Kang, J.; Rui, N.; Hamlyn, R.; Liu, Z.; Orozco, I.; Ramírez, P. J.; Senanayake, S. D.; Rodriguez, J. A., The behavior of inverse oxide/metal catalysts: CO oxidation and water-gas shift reactions over ZnO/Cu(111) surfaces. *Surf. Sci.* **2019,** *681*, 116-121.
31. Mahapatra, M.; Kang, J. D.; Ramiirez, P. J.; Hamlyn, R.; Rui, N.; Liu, Z. Y.; Orozco, I.; Senanayake, S. D.; Rodriguez, J. A., Growth, structure, and catalytic properties of ZnO_x grown on $CuO_x/Cu(111)$ surfaces. *J. Phys. Chem. C* **2018,** *122* (46), 26554-26562.

32. Yang, F.; Choi, Y. M.; Liu, P.; Hrbek, J.; Rodriguez, J. A., Autocatalytic reduction of a Cu_2O/Cu(111) surface by CO: STM, XPS, and DFT studies. *J. Phys. Chem. C* **2010,** *114* (40), 17042-17050.
33. Baber, A. E.; Xu, F.; Dvorak, F.; Mudiyanselage, K.; Soldemo, M.; Weissenrieder, J.; Senanayake, S. D.; Sadowski, J. T.; Rodriguez, J. A.; Matolin, V.; White, M. G.; Stacchiola, D. J., In situ imaging of Cu_2O under reducing conditions: Formation of metallic fronts by mass transfer. *J. Am. Chem. Soc.* **2013,** *135* (45), 16781-16784.
34. Lustemberg, P. G.; Palomino, R. M.; Gutierrez, R. A.; Grinter, D. C.; Vorokhta, M.; Liu, Z.; Ramirez, P. J.; Matolin, V.; Ganduglia-Pirovano, M. V.; Senanayake, S. D.; Rodriguez, J. A., Direct conversion of methane to methanol on Ni-Ceria surfaces: Metal-support interactions and water-enabled catalytic conversion by site blocking. *J. Am. Chem. Soc.* **2018,** *140* (24), 7681-7687.
35. Orozco, I.; Huang, E.; Mahapatra, M.; Kang, J.; Shi, R.; Nemšák, S.; Tong, X.; Senanayake, S. D.; Liu, P.; Rodríguez, J. A., Understanding methanol synthesis on inverse ZnO/CuO_x/Cu catalysts: Stability of CH_3O species and dynamic nature of the surface. *J. Phys. Chem. C* **2021,** *125* (12), 6673-6683.
36. Vohs, J. M.; Barteau, M. A., Conversion of methanol, formaldehyde and formic acid on the polar faces of zinc oxide. *Surf. Sci.* **1986,** *176* (1), 91-114.
37. Hohenberg, P.; Kohn, W., Inhomogeneous electron gas. *Phys. Rev.* **1964,** *136* (3B), B864-B871.
38. Kohn, W.; Sham, L. J., Self-consistent equations including exchange and correlation effects. *Phys. Rev.* **1965,** *140* (4A), A1133-A1138.
39. Kresse, G.; Furthmuller, J., Efficient iterative schemes for ab initio total-energy calculations using a plane-wave basis set. *Phys. Rev. B* **1996,** *54* (16), 11169-11186.
40. Blochl, P. E., Projector augmented-wave method. *Phys. Rev. B* **1994,** *50* (24), 17953-17979.
41. Kresse, G.; Joubert, D., From ultrasoft pseudopotentials to the projector augmented-wave method. *Phys. Rev. B* **1999,** *59* (3), 1758-1775.
42. Perdew, J. P.; Burke, K.; Ernzerhof, M., Generalized gradient approximation made simple. *Phys. Rev. Lett.* **1996,** *77* (18), 3865-3868.
43. Monkhorst, H. J.; Pack, J. D., Special points for Brillouin-zone integrations. *Phys. Rev. B* **1976,** *13* (12), 5188-5192.
44. Henkelman, G.; Jonsson, H., Improved tangent estimate in the nudged elastic band method for finding minimum energy paths and saddle points. *J. Chem. Phys.* **2000,** *113* (22), 9978-9985.
45. Dudarev, S. L.; Botton, G. A.; Savrasov, S. Y.; Humphreys, C. J.; Sutton, A. P., Electron-energy-loss spectra and the structural stability of nickel oxide: An LSDA+U study. *Phys. Rev. B* **1998,** *57* (3), 1505-1509.
46. Zhao, X.; Chen, H.; Wu, H.; Wang, R.; Cui, Y.; Fu, Q.; Yang, F.; Bao, X., Growth of ordered ZnO structures on Au(111) and Cu(111). *Acta Phys. -Chim. Sin.* **2018,** *34* (12), 1373-1380.
47. Thang, H. V.; Tosoni, S.; Pacchioni, G., The epitaxial growth of ZnO films on Cu(111) surface: Thickness dependence. *Appl. Surf. Sci.* **2019,** *483*, 133-139.
48. Lee, J.; Sorescu, D. C.; Deng, X., Tunable lattice constant and band gap of single- and few-layer ZnO. *J. Phys. Chem. Lett.* **2016,** *7* (7), 1335-1340.

49. Campbell, C. T.; Árnadóttir, L.; Sellers, J. R. V., Kinetic prefactors of reactions on solid surfaces. Z. Phys. Chem., 2013; Vol. 227, pp 1435-1454.
50. Gokhale, A. A.; Kandoi, S.; Greeley, J. P.; Mavrikakis, M.; Dumesic, J. A., Molecular-level descriptions of surface chemistry in kinetic models using density functional theory. *Chem. Eng. Sci.* **2004,** *59* (22), 4679-4691.
51. NIST computational chemistry comparison and benchmark database. *http://cccbdb.nist.gov/*, (Accessed September 2020).
52. Jansen, A. P. J., An introduction to Monte Carlo simulations of surface reactions. *Springer-Verlag Berlin Heidelberg*, **2012,** *pp. 73-119*.
53. Zuo, Z.; Liu, S.; Wang, Z.; Liu, C.; Huang, W.; Huang, J.; Liu, P., Dry reforming of methane on single-site Ni/MgO catalysts: Importance of site confinement. *ACS Catal.* **2018**, 9821-9835.

For Table of Contents Only